Title: Targeting CD34+ cells of the inflamed synovial endothelium by guided nanoparticles for the treatment of rheumatoid arthritis.

Authors: Federico Colombo[a], Paolo Durigutto[a], Luca De Maso[a], Stefania Biffi[b], Beatrice Belmonte[c], Claudio Tripodo[c], Romina Oliva[d], Paola Bardini[e], Giada M. Marini[e], Enzo Terreno[e], Gabriele Pozzato[f], Enrico Rampazzo[g], Jessica Bertrand[h], Bernd Feuerstein[i], Jakub Javurek[j], Jana Havrankova[j], Costantino Pitzalis[k], Luis Nuñez[l], Pierluigi Meroni[m], Francesco Tedesco[m], Daniele Sblattero[a], Paolo Macor[a, n].

Affiliations:

[a]Department of Life Sciences, University of Trieste, Trieste, Italy; [b]Institute for Maternal and Child Health-IRCCS "Burlo Garofolo", Trieste, Italy; [c]Department of Human Pathology, University of Palermo, Palermo, Italy; [d]Department of Sciences and Technologies, University Parthenope of Naples, Napoli, Italy; [e]Molecular and Preclinical Imaging Centers, Department of Molecular Biotechnology and Health Sciences, University of Torino, Torino, Italy; [f]Department of Medical, Surgery and Health Sciences, University of Trieste, Trieste, Italy; [g]Department of Chemistry "G. Ciamician", University of Bologna, Bologna, Italy; [h]Department of Orthopaedic Surgery, Otto-von-Guericke University, Magdeburg, Germany; [i]Department of Mechanical Engineering, Magdeburg-Stendal University of Applied Sciences, Magdeburg, Germany; [j]Tescan, Brno, Czech Republic; [k]Centre for Experimental Medicine and Rheumatology, William Harvey Research Institute, Barts and The London School of Medicine and Dentistry, Queen Mary University of London, London, UK; [l]LNK Chemsolutions LLC, Lincoln, NE, USA; [m]IRCCS Istituto Auxologico Italiano, Milan, Italy; [n]Experimental and Clinical Pharmacology Unit, Centro di Riferimento Oncologico di Aviano (CRO) IRCCS.

Corresponding author: Pier Luigi Meroni, Experimental Laboratory of Immunological and Rheumatologic Researches, IRCCS Istituto Auxologico Italiano, Via Zucchi 18, 20095 Cusano Milanino, Milan, Italy; e-mail: pierluigi.meroni@unimi.it

ABSTRACT

Despite the advances in the treatment of rheumatoid arthritis (RA) achieved in the last few years, several patients are diagnosed late, do not respond to or have to stop therapy because of inefficacy and/or toxicity, leaving still a huge unmet need. Tissue-specific strategies have the potential to address some of these issues. The aim of the study is the development of a safe nanotechnology approach for tissue-specific delivery of drugs and diagnostic probes. CD34+ endothelial precursors were addressed in inflamed synovium using targeted biodegradable nanoparticles (tBNPs). These nanostructures were made of poly-lactic acid, poly-caprolactone, and PEG and then coated with a synovial homing peptide. Immunofluorescence analysis clearly demonstrated their capacity to selectively address CD34+ endothelial cells in synovial tissue obtained from human, mouse, and rat. Biodistribution studies in two different animal models of rheumatoid arthritis (antigen-induced arthritis/AIA and collagen-induced arthritis/CIA) confirmed the selective accumulation in inflamed joints but also evidenced the capacity of tBNP to detect early phases of the disease and the preferential liver elimination. The therapeutic effect of methotrexate (MTX)-loaded tBNPs were studied in comparison with conventional MTX doses. MTX-loaded tBNPs prevented and treated CIA and AIA at a lower dose and reduced administration frequency than MTX. Moreover, MTX-loaded tBNP showed a novel mechanism of action, in which the particles target and kill CD34+ endothelial progenitors, preventing neo-angiogenesis and, consequently, synovial inflammation. tBNPs represent a stable and safe platform to develop highly-sensitive imaging and therapeutic approaches in RA targeting specifically synovial neo-angiogenesis to reduce local inflammation.

Graphical abstract
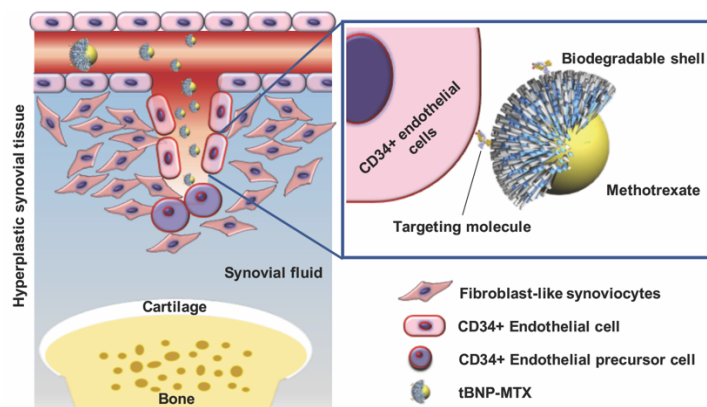
Highlights:
- Targeted nanoparticles highlight early phase of RA inflammation in animal models.
- MTX-loaded targeted nanoparticles-based therapy reduce inflammation in RA animal models with a safe toxicological profile.
- CD34+ precursor endothelial cells are a potential therapeutic target in RA.

Keywords: Rheumatoid Arthritis; Targeted therapy; Targeted Nanoparticles; CD34+ cells; Neoangiogenesis.

1. INTRODUCTION

Rheumatoid arthritis (RA) is a chronic, systemic autoimmune disease affecting joints and extra-articular structures characterized by persistent synovial tissue inflammation[1–3] that leads to joint swelling and pain, as the main clinical symptoms, associated with cartilage damage and bone destruction followed by joint ankylosis[4,5]. The use of disease-modifying anti-rheumatic drugs (DMARDs), in particular methotrexate (MTX)[6,7], and the introduction of biological therapies have significantly improved RA outcomes[8]. Despite the success of these therapeutic approaches, some patients have to stop treatment due to inefficacy or side effects[9,10]. This leads to the discontinuation of therapy[11,12] and indicates the clinical need of new therapeutic targets, but also to improve drug bioavailability in order to decreasing total dose and/or injection frequency with the potential to reduce toxicity and improve compliance to long-term treatment.

Nanotechnology approaches have already been attempted as possible solutions to satisfy these medical needs[13–15] by employing anti-rheumatic drug-encapsulated nanoparticles that exploit the enhanced permeability retention (EPR) effect for their biodistribution[16]. Although this EPR effect increases the concentration of nanoparticles at sites of inflammation where blood vessels are leaky, while the lymphatic system has reduced draining function, it does not ensure selective biodistribution to deliver the contents to pathological tissues only. Guided nanoparticles coated with the peptide RGD, which is capable of targeting the alpha V beta 3 integrin[17–19], have already been investigated in order to circumvent this problem. However, the expression of this integrin is not joint specific[20,21], which consequently allows for extra-articular nanoparticle accumulation[18].

Here, we report the use of targeted biodegradable nanoparticles (tBNPs) functionalized with a cyclic peptide that are able to specifically target the microvasculature of inflamed synovial tissue. The peptide was identified by L. Lee et al.[22] and subsequently developed for selective delivery of recombinant antibodies to inflamed synovial tissue[23]. We demonstrate, in two different animal models, that the tBNPs delivering system is superior to non-functionalized nanoparticles, and able to detect early inflammatory processes otherwise unnoticeable by physical evaluations. Furthermore, MTX-loaded tBNPs were an effective treatment in both animal models, increasing drug bioavailability, allowing reduction in both administration frequency and dosage compared to MTX and thus reducing potential drug toxicity. Lastly, we demonstrated a novel mechanism of action of tBNPs-MTX for RA treatment, which involves the ability of these particles to target CD34+ endothelial cell progenitors, inhibiting their proliferation and therefore blocking the process of neoangiogenesis that is essential to initiate and sustain inflammation in the joints.

2. MATERIALS AND METHODS

2.1 Nanoparticle production

Core-shell biodegradable nanoparticles were produced under class 100 clean-room conditions using a proprietary electrohydrodynamic technology (Bio-Target Inc., Chigaco, IL, USA; LNK Chemsolutions LLC, Lincoln, NE, USA). Their structure was composed of carboxylic acid-terminated biodegradable polymers (PLA-b-PEG-COOH and PCL-COOH). To produce tBNPs, a fraction of PLA-b-PEG-COOH was activated by N-hydroxysuccinimide to conjugate the targeting molecule by exploiting its primary amino groups. The method to produce these nanoparticles was extensively described in the patent US20080187487A1. Briefly, an organic solution containing the polymers of the shell flowed in the external wall of a hollowed tube, while the core fluid containing

MTX (TEVA, UK) flowed in the interior tube. Nanoparticles were formed at the apex of the tube, which was under an electric potential. Nanoparticles produced were then resuspended in an aqueous buffer solution to obtain a stable suspension.

2.2 Statistical analyses

Measures of the mean, standard deviation (SD), standard error of the mean (SEM) and statistical analyses are indicated in each figure legend. P-value of < 0.05 is considered statistically significant.

2.3 Animal models and ethical approval

All the procedures were carried out in accordance with the national and international laws on the use of experimental animals (L.D. 26/2014, Directives 2010/63/EU) and with the ARRIVE guidelines. Sample sizes for all animal experiments were predetermined using G-Power [24] software providing a power of 0.8, 10% signal differences between groups and assuming 5% of SD using two-tailed t-tests. Few animals were excluded from the studies due to a poor arthritis development (in our experience we obtained 80-90% of arthritis incidence) or abnormalities. All the animals were randomly enrolled in the experimental groups and data collected blindly by two operators. Number of animals enrolled in the experiments are indicated in each figure legend.

2.4 AIA model

AIA was induced in male Wistar Hannover rats (Envigo, San Pietro al Natisone, Italy) weighing 120-150g. All the experimental studies have been conducted under total anesthesia by intraperitoneal injection of Zoletil (Virbac, Sintra, Portugal)(25 mg/kg) and Xylazine (Pharmavet, Sassari, Italy)(7.5 mg/kg). The immunization was performed with two intradermic injections (the second one after one week) of 150μg of mBSA (Sigma) in a 0.9% NaCl physiologic solution and emulsified with 200μL of complete Freund adjuvant (CFA) (Sigma). Fourteen days after the second immunization, inflammation was induced by injecting 100μg of mBSA (diluted in 100μL of physiologic solution) in the intraarticular right knee of the rats [25]. The contralateral knee joint was injected with physiological solution as a control.

To verify that rats enrolled in the study developed an immune response against mBSA, an ELISA was used. mBSA (Sigma, 5μg/mL, 100μL/well) was used for well 4μm. Plate was blocked with 2% skim milk in PBS before incubation with serum samples (diluted 1:2000). Rat IgG binding was analyzed using biotin-labeled rabbit anti-rat (Dako, Santa Clara, USA-1:4000), horseradish peroxidase-conjugated streptavidin (Sigma-1:2000) and 3,3′,5,5′-tetramethylbenzidine (TMB) (Sigma).

2.5 Study of particle distribution in the AIA rat model

The Explore Optix MX pre-clinical optical imaging system (GE Healthcare) equipped with a pulsed laser diode and a time-correlated single-photon detector was used to evaluate the biodistribution of 4.8nmol of BNPs-Cy5.5 and tBNPs-Cy5.5 diluted in physiologic solution injected in the tail vein 2 hours after the intraarticular injection of mBSA. A blank image was acquired before intravenous injection of labeled nanoparticles. The animals were monitored at multiple time points using a 670nm pulsed laser diode with a repetition frequency of 80MHz and a time resolution of 12 light pulses. Fluorescence emission was collected at 700nm and detected through a fast photomultiplier tube and a highly sensitive time-correlated single-photon counting system. Two-dimensional scanning regions of interest were selected and laser power, integration time and scan step were optimized according to the signal emitted. The data were recorded as

temporal point-spread functions, and the images have been reconstructed as fluorescence intensity and fluorescence lifetime. After 23 days, the animals were euthanized under total anesthesia. The organs were finally analyzed ex vivo and then embedded in biocompatible gelatinous matrix Tissue Tek OCT (BioOptica, Milano, Italy) and stored at -80°C. Blood samples were collected for subsequent analysis.

2.6 Therapeutic efficacy in the AIA rat model

MTX (1mg/kg/day) and tBNPs-MTX diluted in physiologic solution were administered i.p. in rats developing AIA. The swelling of the knees was measured with a caliper. At the end of the study, animals were euthanized under total anesthesia, and the articular cavities of the right and left knees were washed with PBS (2mL) in order to collect synovial fluids and infiltrated cells. Part of the synovial membranes was collected, embedded in Tissue Tek OCT and stored at -80°C, while the whole articulation was embedded in paraffin for histological analysis. Blood samples were collected for subsequent analysis.

2.7 CIA animal model

Male DBA/1OlaHsd mice (7 weeks old, Envigo) were housed in a temperature and humidity-controlled facility with a 12-hour light/dark cycle and with water and food freely available throughout the experimental period.
Arthritis was induced by immunization with type II collagen (Chondrex Inc., Redmond, WA, USA) dissolved in 10mM acetic acid and emulsified with a 1/1 v/v of complete Freund adjuvant, as described by Brand et al[26]. Each mouse was anesthetized with 3-4% Sevoflurane gas (O_2 95.0%). Mice were immunized at day 0 with 50μL of type II collagen and were boosted with the same antigen at day 15. The progression of CIA was evaluated by macroscopic scoring 3 times per week. A numeric score was applied for each paw using the following scale (0: no inflammation; 4: severe inflammation): 0 = no evidence of erythema and swelling, 1 = erythema and mild swelling confined to the tarsals or ankle joint, 2 = erythema and mild swelling extending from the ankle to the tarsals, 3 = erythema and moderate swelling extending from the ankle to metatarsal joints, and 4 = erythema and severe swelling encompassing the ankle, foot and digits, or ankyloses of the limb. An ELISA was performed in order to verify that all mice enrolled in the study developed an immune response against bovine collagen type II.

2.8 Study of particle distribution in the CIA mouse model

On day 28, after the first immunization with type II collagen, two groups received in the tail vein BNPs-Cy5.5 (0.5 nmol Cy5.5/mouse) as a control compound (n= 3) or the same amount of tBNPs-Cy5.5 (n= 4). Optical imaging acquisitions were performed before these injections and at the following time points post injection: 1, 6, 24, 72, 96, and 168 hours. IVIS® Spectrum (Perkin Elmer Inc., USA) was used for image acquisition (excitation wavelength at 675nm and emission at 720nm), and illumination settings were as follows: f-stop 2, field of views 6.6, binning medium, acquisition time 1 second (time points of 1, 6, 24, and 72 hours) or 15 seconds (time points of 96 and 168 hours). Images were acquired and analyzed with Living Image Software (Caliper Life Sciences).
All the animals were anesthetized under 3-4% Sevoflurane gas (O_2 95.0%). A region of interest was drawn by the operator over each paw of the mouse, and data were collected as radiant efficiency values. The fluorescent signal value was obtained by subtracting the radiant efficiency value measured before the injection from the signal measured post injection.

2.9 Therapeutic efficacy in the CIA mouse model

Five different groups of CIA mice (scores of 2-3) received: saline, MTX 1mg/kg/3 times per week or 3mg/kg/once per week, tBNPs-MTX 3mg/kg/once per week or 1mg/kg/once per week. All the treatments were administered i.p. for 25 days. Animals were then euthanized under total anesthesia with Zoletil (Virbac-25 mg/kg) and Xylazine (Pharmatech-7.5 mg/kg). The paws, brain, liver, kidneys, spleen, lungs and heart were embedded in Tissue Tek OCT (BioOptica) and stored at -80°C, except for the paws, which were previously fixed in 10% neutral buffered-formalin (BioOptica) for 24 hours and then decalcified for 24 hours with Decalcifying Solution-Lite (Sigma). Blood samples were collected for subsequent analyses.

3   RESULTS

3.1 Design and structural characterization of biodegradable nanoparticles

To prepare the tBNPs we initially generated a targeting molecule that consists of a synovial homing peptide fused to a scFv-Fc (single chain fragment variable – fragment crystallizable) (Fig. 1A). More specifically, the synovial homing peptide was made of 9 amino acids (CKSTHDRLC) containing two flanking cysteines (Fig. 1A), which constrain the peptide in a circular shape. Coomassie staining and western blot analysis of the molecule (Fig. 1B-C) revealed the expected molecular weight (62 kDa) and absence of contaminations or protein degradation.

Immunofluorescence analysis of rat synovial tissues incubated with the targeting molecule confirms our previous finding that it binds to inflamed synovium but not to the normal tissue (Fig. S1). Since the synovial homing peptide was first reported to bind preferentially inflamed RA synovial vasculature, synovial tissues from RA patients were double stained with both the targeting molecule and von Willebrand Factor (vWF) as a marker of endothelial cells (Fig. 2A). The results show diverse co-staining with some vessels positive for both markers, while others stained for either vWF or the targeting molecule, which was also detected on isolated cells (Fig. 2B). Interestingly, staining of the synovial tissue for CD34, which is highly expressed on vascular endothelial progenitors[27,28], revealed a strong co-localization between the targeting molecule and CD34+ cells (Fig. 2C-E). In particular, CD34+ cells were bound by the targeting molecule in close proximity to blood vessels.

The targeting molecule was used to produce two different types of core-shell BNPs made of COOH-poly(ethylene glycol)-b-polylactide (PEG-b-PLA) and poly(caprolactone)-COOH (PCL)[29,30], one of which was loaded with MTX (tBNPs-MTX), while the other contained an empty core (tBNPs). Two additional types of untargeted nanoparticles containing either an empty core (BNPs) or MTX (BNPs-MTX) were generated and used as controls (Fig. 3A).

The 3D structure of the targeting molecule was modeled in silico to predict its possible orientation on the surface of the nanoparticles. In the obtained model, some primary amino groups are exposed on the molecule surface and are available for covalent binding to the nanoparticle. In Fig. 3A, three possible sites for the binding of scFv-Fc to the nanoparticle are schematically shown, corresponding to the most solvent accessible primary amines (the side chains of Lys355 and Lys369 in the Fc-CH2 domain, and the protein N-terminus). All these sites are far from the targeting peptide and are compatible with its exposure on the particle surface and, consequently, with its availability for interaction with synovial tissue.

These nanoparticles were investigated by NanoTrack analysis (Fig. 3B), which showed homogeneous average hydrodynamic diameters ($\approx$ 170 nm) and monodispersity (PdI $\approx$ 0.2) and a very similar nanoparticle concentration (approximately 10^{10}/mL). These results were in line with the ones obtained by dynamic light scattering (DLS, Fig. 3C). A slightly negative ζ-potential (-8

mV) was measured for all the samples. Moreover, the particle showed a round shape and a uniform polymer distribution in both transmission electron microscopy (TEM, Fig. 3D) and scanning transmission electron microscopy (STEM, Fig. 3E-F).

To further characterize the structure of MTX-loaded BNPs, we analyzed the spontaneous release of MTX from the nanoparticles, showing that, after an initial burst release in which 40% of the MTX is dispersed from the tBNPs, more than 50% of the MTX was stably encapsulated for 24 hours (Fig. 3G). The same results were obtained when analyzing particles stored at -20°C for 1 year, demonstrating the stability of the nanosystems and suggesting that nanoparticles, once injected and delivered to the target, would release 50% of the drug over a period longer than 24 hours (data not shown).

3.2 Functional characterization of tBNPs

The functional characterization of the BNPs started in vitro using the EA.hy926 cell line that expresses the synovial homing peptide target. These cells incubated with fluorescently labeled BNPs and tBNPs were followed for 3 hours by live imaging microscopy (example in Video S1) in order to investigate their interaction with tBNPs. To assess this, the binding time of BNPs or tBNPs with endothelial cells was calculated through tracking analysis. After 1 hour (Fig. 4A), an increased time of interaction was reported for the tBNPs compared to BNPs. Similar results were obtained after 3 hours (Fig. 4B). These data were confirmed by ELISA, in which we incubated endothelial cells with both nanosystems for 1 hour (Fig. 4C). Finally, tBNPs were visualized inside EA.hy926 cells by confocal microscopy analysis, proving that tBNPs are already internalized after 1h of incubation (Fig. 4D and Video S2). Binding and internalization of tBNPs-MTX were found to cause the death of endothelial cells to an increased degree over free MTX, and most importantly, residual MTX that remained in the BNPs after dialysis was still able to induce the same extent of endothelial cell death (Fig. 4E).

The superior cell binding of fluorescent tBNPs was confirmed in rat synovial tissues, where stronger staining was found with tBNPs in inflamed synovium than in either non-inflamed synovial tissues or untargeted particles (Fig. S2).

3.3 Biodistribution of tBNPs in animal models of arthritis

After completing the *in vitro* characterization, tBNP behavior was studied in two animal models of RA. First, the biodistribution of tBNPs and BNPs was compared in a rat antigen-induced arthritis (AIA) model, in which monoarthritis is induced in the right knee using the left knee as control. Three days after the induction of inflammation, Cy5.5-labeled tBNPs or BNPs were injected into the animals' tail vein, and their biodistribution was followed for 23 days (Fig. 5A). The animals were scanned by near-infrared optical imaging, and a higher accumulation of fluorescent nanoparticles was observed in the right knee of animals receiving tBNPs-Cy5.5 compared to the contralateral non-inflamed knee or to the inflamed knee of animals treated with BNPs-Cy5.5. Measuring the fluorescence intensity at various time points, a progressive accumulation of tBNPs-Cy5.5 was observed in the inflamed joints, reaching a maximum value after 7-8 days (Fig. 5B). The localization of both tBNPs-Cy5.5 and BNPs-Cy5.5 in the non-inflamed left knee was negligible (Fig. 5B). The fluorescence intensity detected in the knees was related to the joint swelling (Fig. 5C) and was used as a marker to evaluate inflammation in AIA. It is important to note that both groups of animals receiving the two types of nanoparticles showed the same degree of knee swelling (Fig. 5C) as a consequence of a similar IgG response to bovine serum albumin (BSA) (Fig. S3).

To analyze particle clearance, residual fluorescence was measured at the end of the experiment in the paws and in the main organs, including the kidneys, liver, lungs, brain, heart and spleen. The results presented in Fig. 5D show an increased accumulation of nanoparticles in the liver, while low intensity of fluorescence was detected in the other main organs.

The biodistribution of tBNPs was then tested in collagen-induced arthritis (CIA), which shares several features with human RA, involving most joints, and is considered the gold standard to test new compounds at pre-clinical level for the imaging and treatment of RA. Two groups of mice showing similar signs of arthritis received either tBNPs-Cy5.5 or BNPs-Cy5.5 into their tail veins. The animals were scanned for 7 days, and the images of the limbs of two representative mice are presented in Fig. 6A. To correlate the fluorescence intensity with the degree of joint inflammation, disease severity was measured by assigning an arthritis score ranging from 0 (no arthritis) to 4 (severe arthritis). Interestingly, paws with the same scores in the two groups of mice showed different fluorescence intensities, and the highest level was detected in the paws of mice 24 hours after injection of either type of nanoparticle (Fig. 6B). Surprisingly, an increased presence of tBNPs was also observed in paws with a score of 0, which should not be inflamed. Histological analysis of these samples, however, indicated features of an early inflammatory process, such as leukocyte infiltration (Fig. 6C).

3.4 Treatment of CIA using MTX-loaded tBNPs

Having established the selective delivery of tBNPs to inflamed synovia, we sought to determine whether MTX-loaded targeted nanoparticles were able to control the development of CIA in mice treated weekly for 3 weeks and followed for 25 days after disease onset. To this end, one group of mice was treated with collagen to induce arthritis and was then administered a single weekly injection of 3 mg/kg tBNPs-MTX that resulted in substantial amelioration of the joint inflammation and reduced arthritis progression compared to saline-treated animals (Fig. 7A). Similar beneficial effects were obtained in mice that received 1 mg/kg of free MTX three times a week, while a single injection of 3 mg/kg of free MTX was ineffective (Fig. 7A). The timing and dosing of free MTX administration were critical for efficacy because the drug is cleared rapidly with a half-life of 34 minutes[31]. In contrast, the persistence of the nanoparticles in the inflamed synovium for approximately a week explains the beneficial effects associated with a single injection of tBNPs-MTX. Interestingly, tBNPs-MTX also proved to be therapeutically effective at a single dose of 1 mg/kg per week (Fig. 7A).

As shown in Fig. 7B, histological analysis of the joints from treated animals indicated reduced leukocyte infiltration and bone degradation. Histological scores of the inflammatory parameters, summarized in Fig. S4, revealed a reduction in cartilage and subchondral bone leukocyte infiltration as well as decreased stromal cell proliferation in mice treated with a single weekly injection of tBNPs-MTX.

We have also evaluated the potential toxic effects of tBNPs-MTX compared to the free drug by analyzing body weight and changes in blood cell counts in the treated animals. Injection of tBNPs-MTX did not affect body weight, whereas free MTX administered once a week at the dose of 3 mg/kg caused a 60% reduction in mice growth (Fig. 7C), despite its failure to produce a therapeutic effect. Likewise, red blood cell, leukocyte and platelet counts (Fig. 7D-F) in mice treated with tBNPs-MTX did not change, while mice receiving 1 mg/kg of free MTX three times a week presented a significant decrease in the red blood cell and platelet counts. Subsequently, morphological analysis of various organs of the specimens highlighted heterogeneous tissue damage related to the treatment toxicity in mice treated with saline, tBNPs-MTX, or free MTX. In all treatment conditions, the specimens presented a disarray of the pulmonary parenchyma

consisting of a variable grade of increased interstitial cellularity and fibrosis as well as blood extravasation. A variable grade of decreased cortical glomerular density or rarefaction associated with necrosis, rarely also involving the tubules, was detected in the renal parenchyma. Both the histopathological alterations observed in the lung and kidney presented at a higher severity in free MTX samples than in tBNPs-MTX samples (Fig. S5A). No significant histopathological alterations of the liver, spleen, brain or heart were detected in any of the treatment conditions (Fig. S5B).

3.5 Treatment of AIA using MTX-loaded tBNPs to prevent neoangiogenesis
To investigate the mechanism of action of MTX-tBNPs we turn again to the AIA model. MTX-tBNPs, unlike free MTX, reduced knee swelling and the number of polymorphonuclear (PMN) cells in the synovial fluid compared to controls (Fig. 8A and B). The treated rats did not show any sign of toxicity (Fig. S6) and had levels of anti-methylated BSA (mBSA) IgG and C3 deposition in synovial tissues that were comparable to the controls (Fig. S7A and B), thus ruling out differences in the induction of the inflammatory model between the two groups of rats.

Taking into account that tBNPs target endothelial cell precursors, it was reasonable to investigate their effect on the control of neoangiogenesis, which is usually associated with joint inflammation in these models and in RA patients[32]. To this end, synovial tissues obtained from untreated animals or animals treated with free MTX or tBNPs-MTX were stained for the vWF to visualize the vessels. Representative figures are shown in Fig. S8. The vessel density data, expressed as intensity of vWF fluorescence/tissue area and summarized in Fig. 8C, show a reduced number of vessels in rats treated with tBNPs-MTX compared to both control- and MTX-treated rats, supporting the hypothesis that tBNPs-MTX interfere with the formation of new vessels in inflamed synovia. Given the above demonstrated binding of tBNPs to CD34+ cells, it is tempting to conclude that the selective delivery of MTX to CD34+ endothelial cells precursors causes cell death, preventing the development of new vessels in the inflamed synovial tissue and the local recruitment of leukocytes (Fig. 8D).

4   DISCUSSION

Efforts are being made to develop diagnostic and therapeutic approaches that preferentially localize to tissues principally affected by the pathologic process. This was mainly proposed for cancer treatment, but this strategy was also described for the treatment of rheumatoid arthritis, with the aim to locally inhibit effector molecules usually present in the circulation and in the body fluids. The selective delivery of mAbs [23] initially showed the potential validity of this approach as well as the selective delivery of chemical drugs using guided nanoparticles coated with the peptide RGD [17], though the expression of the alpha V beta 3 integrin is not tissue specific and cause an extra-articular nanoparticle accumulation [17].

The treatment of RA remains anchored to the use of MTX and biological drugs, although some patients have to stop treatments due to their side effects [33], leaving the management of RA still problematic. For this reason, the development of novel therapeutic approaches targeting different mechanisms of action from standard drugs are desirable. Although the autoimmune response in RA patients is triggered at various organs and that systemic treatments clearly demonstrated their efficacy, the pathogenic paths driving inflammation take place in the synovial tissues, and therefore their specific control remains a priority.

Here, we present a novel drug delivery system for the management of rheumatoid arthritis. It is based on the use of drug-loaded polymeric biodegradable nanoparticles functionalized with a

targeting agent specific for endothelial cells precursors in the inflamed synovial tissue. We demonstrated that such treatment blocks the progression of the inflammatory process through inhibition of tissue-specific neoangiogenesis.

Several types of structures have been previously proposed for drug delivery. Each of them has been extensively characterized in vitro for their physicochemical properties. tBNPs solutions, developed in this study are monodisperse and stable for long-term storage. The drug release showed that after an initial burst release, a described phenomenon associated with the shape and pore size of the polymeric nanoparticles[34], in which 40% of the MTX is dispersed from the tBNPs, ≈50% of MTX is still encapsulated after 24 hours. This data results particularly important because demonstrated the capacity of residual loaded drug to kill endothelial cells even after 24 hours of distribution in the body.

Particular attention was also devoted to the characterization of the targeting agent. *In silico* studies showed the three most probable orientations of the targeting molecule on the surface of the nanoparticles, all ensuring the exposure of the synovial peptide far from the nanoparticles surface and from PEG branches. These predictions were confirmed by immunofluorescence staining between tBNPs and inflamed rat synovial tissues demonstrating that the targeting agent is needed to specifically target the inflamed synovial membrane and confirming nanoparticles functionalization. In addition, as demonstrated by tracking analysis studies, we found that the targeting agent is important to increase the time of interaction between tBNPs and endothelial cells, emphasizing the important role of the targeting peptide at the beginning of the interaction. This finding suggests that even *in vivo* the retention time of tBNPs is increased compared to BNPs. In order to determine the specific binding of the synovial peptide, the targeting molecule was stained in combination with endothelial markers, such as vWF and CD34. A colocalization with the CD34+ was detected on inflamed human synovial membranes; in particular, many individual CD34+ cells were recognized by the targeting molecule in close proximity to blood vessels. This staining pattern has been previously reported[35,36], demonstrating the great variability in the expression and distribution of endothelial cell markers among different types of vascular tissues and different anatomic compartments. These findings confirmed that the synovial peptide exploits its target as a signature of the inflamed synovial membrane, highlighting its potentiality as a disease-specific targeting agent.

Through the biodistribution studies conducted in AIA, we demonstrated that targeted tBNPs were found to be more efficient than untargeted particles in discriminating between inflamed and non-inflamed joints, further supporting the conclusion that the higher tBNP accumulation in the inflamed knee was the result of active targeting. At the end of this study, we measured the residual amount of nanoparticles in other organs, confirming data obtained with similar particles by our group[29,37] and indicating that the structures are mainly cleared through the liver, bile and intestine. The undetectable presence of nanoparticles in the lungs confirmed that our nanosystems are not non-specifically bound by macrophages.

Moreover, this study shows an increased accumulation of tBNPs into inflamed joints of mice that, even though were scored as 0, present tracts of an early inflammatory process by histological analysis. For this reason, these data underline the potential use of tBNPs as a diagnostic tool able to reveal inflammatory processes that cannot be detected by physical examination. These results obtained *in vivo* prove again the superior accumulation of targeted nanoparticles compared with untargeted nanoparticles and demonstrate that the targeting molecule actively guides nanoparticles to inflamed joints. Moreover, this is a further proof that the use of targeted nanoparticles is a

potential way to overcome the lack of efficacy of untargeted nanocarriers based on passive delivery.

CIA represent the animal model sharing more features with chronic human pathology. The treatment with MTX-loaded tBNPs reduced the severity of the disease compared to control animals. In particular, a lower dose of tBNPs-MTX maintains its efficacy compared to the same dose of the free drug. These results confirmed the initial hypothesis that, through targeted delivery system, it is possible to increased drug bioavailability at the disease site, while reducing systemic side toxicity secondary to decrease in dose reduction and administration frequency. Indeed, no toxic effects were associated with tBNPs-MTX treatment while mice receiving the standard dose of MTX three times a week presented a significant decrease in the red blood cell and platelet counts. These data confirm previous observations of cytopenia associated with frequent injections of MTX[33,38].

Based on our finding that tBNPs are able to deliver MTX inside CD34+ cells in synovial tissue and considering that different regimens of free MTX and MTX-loaded tBNPs were needed to obtain similar results in the treatment of CIA, we hypothesized that free MTX and MTX-loaded tBNPs may have different mechanisms of action. To address this point, we used the AIA model, which is dependent on the production of immune complexes in the joint microenvironment; this production in turn activates the complement system, eventually leading to recruitment of immune cells[23,39]. This model develops in 3-4 days and is unresponsive to free MTX[40,41] due to the insufficient time that MTX has to inhibit the production of antibodies that initiate the inflammatory process. MTX-tBNPs demonstrated their capacity to completely prevent inflammation in this acute model of arthritis where free MTX was ineffective. This result was not dependent on immune-complexes deposition or complement activation but to the capacity to target CD34+ endothelial cell precursor, preventing neo-angiogenesis specifically at synovial sites and, as a consequence, inflammatory cell migration from the circulation.

5   CONCLUSIONS

We present data in support of a novel approach for the treatment of RA through the use of polymeric nanoparticles that block neoangiogenesis only in an inflamed synovial microenvironment. The MTX-loaded targeted nanoparticles generated in this study have the great advantage of delivering the drug to inflamed synovia using the synovium-homing peptide as a targeting molecule. This approach allows the local release of the smallest amount of MTX sufficient to be therapeutically effective, while minimizing side effects by reducing systemic toxicity.

6   ACKNOWLEDGMENTS

7   REFERENCES

[1]   J.S. Smolen, D. Aletaha, I.B. McInnes, Rheumatoid arthritis, Lancet. 388 (2016) 2023–2038. doi:10.1016/S0140-6736(16)30173-8.

[2]   I.B. McInnes, G. Schett, The Pathogenesis of Rheumatoid Arthritis, N. Engl. J. Med. 365 (2011) 2205–2219. doi:10.1056/NEJMra1004965.

[3]   D. Aletaha, T. Neogi, A.J. Silman, J. Funovits, D.T. Felson, C.O. Bingham 3rd, N.S. Birnbaum, G.R. Burmester, V.P. Bykerk, M.D. Cohen, B. Combe, K.H. Costenbader, M. Dougados, P. Emery, G. Ferraccioli, J.M. Hazes, K. Hobbs, T.W. Huizinga, A. Kavanaugh, J. Kay, T.K. Kvien, T. Laing, P. Mease, H.A. Menard, L.W. Moreland, R.L. Naden, T. Pincus, J.S. Smolen, E. Stanislawska-Biernat, D. Symmons, P.P. Tak, K.S. Upchurch, J. Vencovsky, F. Wolfe, G. Hawker, 2010 Rheumatoid arthritis classification criteria: an American College of Rheumatology/European League Against Rheumatism collaborative initiative, Arthritis Rheum. 62 (2010) 2569–2581. doi:10.1002/art.27584.

[4]   J.S. Smolen, D. Aletaha, M. Koeller, M.H. Weisman, P. Emery, New therapies for treatment of rheumatoid arthritis, Lancet. 370 (2007) 1861–1874. doi:10.1016/S0140-6736(07)60784-3.

[5]   J.S. Smolen, D. Aletaha, A. Barton, G.R. Burmester, P. Emery, G.S. Firestein, A. Kavanaugh, I.B. McInnes, D.H. Solomon, V. Strand, K. Yamamoto, Rheumatoid arthritis, Nat. Rev. Dis. Prim. 4 (2018). doi:10.1038/nrdp.2018.1.

[6]   T. Pincus, Y. Yazici, T. Sokka, D. Aletaha, J.S. Smolen, Methotrexate as the "anchor drug" for the treatment of early rheumatoid arthritis, Clin. Exp. Rheumatol. 21 (2003) S179–185.

[7]   E.G. Favalli, M. Biggioggero, P.L. Meroni, Methotrexate for the treatment of rheumatoid arthritis in the biologic era: Still an "anchor" drug?, Autoimmun. Rev. 13 (2014) 1102–1108. doi:10.1016/j.autrev.2014.08.026.

[8]   R.F. Van Vollenhoven, Treatment of rheumatoid arthritis: State of the art 2009, Nat. Rev. Rheumatol. 5 (2009) 531–541. doi:10.1038/nrrheum.2009.182.

[9]   J.W. Van Der Heijden, B. a C. Dijkmans, R.J. Scheper, G. Jansen, Drug Insight: resistance to methotrexate and other disease-modifying antirheumatic drugs--from bench to bedside., Nat. Clin. Pract. Rheumatol. 3 (2007) 26–34. doi:10.1038/ncprheum0380.

[10]   V.C. Romão, A. Lima, M. Bernardes, H. Canhão, J.E. Fonseca, Three decades of low-dose methotrexate in rheumatoid arthritis: Can we predict toxicity?, Immunol. Res. 60 (2014) 289–310. doi:10.1007/s12026-014-8564-6.

[11]   E. Lie, D. Der Van Heijde, T. Uhlig, M.S. Heiberg, W. Koldingsnes, E. Rødevand, C. Kaufmann, K. Mikkelsen, T.K. Kvien, Effectiveness and retention rates of methotrexate in psoriatic arthritis in comparison with methotrexate-treated patients with rheumatoid arthritis, Ann. Rheum. Dis. 69 (2010) 671–676. doi:10.1136/ard.2009.113308.

[12]   P.M. Brown, A.G. Pratt, J.D. Isaacs, Mechanism of action of methotrexate in rheumatoid arthritis, and the search for biomarkers, Nat. Rev. Rheumatol. 12 (2016) 731–742. doi:10.1038/nrrheum.2016.175.

[13]   M. Ferrari, S.C. Onuoha, C. Pitzalis, Trojan horses and guided missiles: targeted therapies in the war on arthritis, Nat. Rev. Rheumatol. 11 (2015) 328–337. doi:10.1038/nrrheum.2015.17.

[14]   P. Prabhu, R. Shetty, M. Koland, K. Vijayanarayana, K.K. Vijayalakshmi, M.H. Nairy, G.S. Nisha, Investigation of nano lipid vesicles of methotrexate for anti-rheumatoid activity, Int. J. Nanomedicine. 7 (2012) 177–186. doi:10.2147/IJN.S25310.

[15] Y.S. Jung, W. Park, K. Na, Temperature-modulated noncovalent interaction controllable complex for the long-term delivery of etanercept to treat rheumatoid arthritis, J. Control. Release. 171 (2013) 143–151. doi:10.1016/j.jconrel.2013.07.012.

[16] H. Maeda, H. Nakamura, J. Fang, The EPR effect for macromolecular drug delivery to solid tumors: Improvement of tumor uptake, lowering of systemic toxicity, and distinct tumor imaging in vivo, Adv. Drug Deliv. Rev. 65 (2013) 71–79. doi:10.1016/j.addr.2012.10.002.

[17] S.M. Lee, H.J. Kim, Y.J. Ha, Y.N. Park, S.K. Lee, Y.B. Park, K.H. Yoo, Targeted chemo-photothermal treatments of rheumatoid arthritis using gold half-shell multifunctional nanoparticles, ACS Nano. 7 (2013) 50–57. doi:10.1021/nn301215q.

[18] R.I. Scheinman, R. Trivedi, S. Vermillion, U.B. Kompella, Functionalized STAT1 siRNA nanoparticles regress rheumatoid arthritis in a mouse model, Nanomedicine. 6 (2011) 1669–1682. doi:10.2217/nnm.11.90.

[19] A.S. Vanniasinghe, N. Manolios, S. Schibeci, C. Lakhiani, E. Kamali-Sarvestani, R. Sharma, V. Kumar, M. Moghaddam, M. Ali, V. Bender, Targeting fibroblast-like synovial cells at sites of inflammation with peptide targeted liposomes results in inhibition of experimental arthritis, Clin. Immunol. 151 (2014) 43–54. doi:10.1016/j.clim.2014.01.005.

[20] R.L. Wilder, Integrin alpha V beta 3 as a target for treatment of rheumatoid arthritis and related rheumatic diseases., Ann. Rheum. Dis. 61 Suppl 2 (2002) ii96-9. doi:10.1136/ard.61.suppl_2.ii96.

[21] P. Durigutto, D. Sblattero, S. Biffi, L. De Maso, C. Garrovo, G. Baj, F. Colombo, F. Fischetti, A.F. Di Naro, F. Tedesco, P. Macor, Targeted delivery of neutralizing anti-C5 antibody to renal endothelium prevents complement- dependent tissue damage, Front. Immunol. 8 (2017). doi:10.3389/fimmu.2017.01093.

[22] L. Lee, C. Buckley, M.C. Blades, G. Panayi, A.J. George, C. Pitzalis, Identification of synovium-specific homing peptides by in vivo phage display selection, Arthritis Rheum. 46 (2002) 2109–2120. doi:10.1002/art.10464.

[23] P. Macor, P. Durigutto, L. De Maso, C. Garrovo, S. Biffi, A. Cortini, F. Fischetti, D. Sblattero, C. Pitzalis, R. Marzari, F. Tedesco, Treatment of experimental arthritis by targeting synovial endothelium with a neutralizing recombinant antibody to C5, Arthritis Rheum. 64 (2012) 2559–2567. doi:10.1002/art.34430.

[24] E. Erdfelder, F. Faul, A. Buchner, A.A.-G. Lang, Franz Faul Edgar Erdfelder and Albert-georg Lang and Axel Buchner, Statistical power analyses using G*Power 3.1: test for correlation and regression analyses, Behav. Res. Methods. 41 (2009) 1149–1160. doi:10.3758/BRM.41.4.1149.

[25] S. Donato, S. Pacilè, F. Colombo, C. Garrovo, S.D. Monego, P. Macor, G. Tromba, S. Biffi, Meniscal ossicles as micro-CT imaging biomarker in a rodent model of antigen-induced arthritis: A synchrotron-based x-ray pilot study, Sci. Rep. 7 (2017). doi:10.1038/s41598-017-08025-7.

[26] D.D. Brand, K.A. Latham, E.F. Rosloniec, Collagen-induced arthritis, Nat. Protoc. 2 (2007) 1269–1275. doi:10.1038/nprot.2007.173.

[27] D.S. Krause, M.J. Fackler, C.I. Civin, W.S. May, CD34: structure, biology, and clinical utility., Blood. 87 (1996) 1–13.

[28] L.E. Sidney, M.J. Branch, S.E. Dunphy, H.S. Dua, A. Hopkinson, Concise review: Evidence for CD34 as a common marker for diverse progenitors, Stem Cells. 32 (2014) 1380–1389. doi:10.1002/stem.1661.

[29] S. Capolla, C. Garrovo, S. Zorzet, A. Lorenzon, E. Rampazzo, R. Spretz, G. Pozzato, L. Núñez, C. Tripodo, P. Macor, S. Biffi, Targeted tumor imaging of anti-CD20-polymeric nanoparticles developed for the diagnosis of B-cell malignancies, Int. J. Nanomedicine. 10 (2015) 4099–4109. doi:10.2147/IJN.S78995.

[30] N. Mezzaroba, S. Zorzet, E. Secco, S. Biffi, C. Tripodo, M. Calvaruso, R. Mendoza-Maldonado, S. Capolla, M. Granzotto, R. Spretz, G. Larsen, S. Noriega, M. Lucafò, E. Mansilla, C. Garrovo, G.H. Marín, G. Baj, V. Gattei, G. Pozzato, L. Núñez, P. Macor, New Potential Therapeutic Approach for the Treatment of B-Cell Malignancies Using Chlorambucil/Hydroxychloroquine-Loaded Anti-CD20 Nanoparticles, PLoS One. 8 (2013) e74216. doi:10.1371/journal.pone.0074216.

[31] E.D. Lobo, J.P. Balthasar, Pharmacokinetic-pharmacodynamic modeling of methotrexate-induced toxicity in mice, J. Pharm. Sci. 92 (2003) 1654–1664. doi:10.1002/jps.10431.

[32] A.W. Mould, I.D. Tonks, M.M. Cahill, A.R. Pettit, R. Thomas, N.K. Hayward, G.F. Kay, Vegfb gene knockout mice display reduced pathology and synovial angiogenesis in both antigen-induced and collagen-induced models of arthritis, Arthritis Rheum. 48 (2003) 2660–2669. doi:10.1002/art.11232.

[33] C. Salliot, D. Van Der Heijde, Long-term safety of methotrexate monotherapy in patients with rheumatoid arthritis: A systematic literature research, Ann. Rheum. Dis. 68 (2009) 1100–1104. doi:10.1136/ard.2008.093690.

[34] X. Huang, C.S. Brazel, On the importance and mechanisms of burst release in matrix-controlled drug delivery systems, J. Control. Release. 73 (2001) 121–136. doi:10.1016/S0168-3659(01)00248-6.

[35] M.P. Pusztaszeri, W. Seelentag, F.T. Bosman, Immunohistochemical Expression of Endothelial Markers CD31, CD34, von Willebrand Factor, and Fli-1 in Normal Human Tissues, J. Histochem. Cytochem. 54 (2006) 385–395. doi:10.1369/jhc.4A6514.2005.

[36] B. Rüger, A. Giurea, A.H. Wanivenhaus, H. Zehetgruber, D. Hollemann, G. Yanagida, M. Groger, P. Petzelbauer, J.S. Smolen, P. Hoecker, M.B. Fischer, Endothelial precursor cells in the synovial tissue of patients with rheumatoid arthritis and osteoarthritis, Arthritis Rheum. 50 (2004) 2157–2166. doi:10.1002/art.20506.

[37] S. Capolla, N. Mezzaroba, S. Zorzet, C. Tripodo, R. Mendoza-Maldonado, M. Granzotto, F. Vita, R. Spretz, G. Larsen, S. Noriega, E. Mansilla, M. Dal Bo, V. Gattei, G. Pozzato, L. Núñez, P. Macor, A new approach for the treatment of CLL using chlorambucil/hydroxychloroquine-loaded anti-CD20 nanoparticles, Nano Res. 9 (2016) 537–548. doi:10.1007/s12274-015-0935-3.

[38] R. Rau, G. Herborn, Benefit and risk of methotrexate treatment in rheumatoid arthritis, Clin. Exp. Rheumatol. 22 (2004) S83–S94.

[39] P. Durigutto, P. Macor, F. Ziller, L. De Maso, F. Fischetti, R. Marzari, D. Sblattero, F. Tedesco, Prevention of arthritis by locally synthesized recombinant antibody neutralizing complement component C5, PLoS One. 8 (2013) e58696. doi:10.1371/journal.pone.0058696.

[40] A.S. Williams, J.P. Camilleri, R.M. Goodfellow, B.D. Williams, A single intra-articular injection of liposomally conjugated methotrexate suppresses joint inflammation in rat antigen-induced arthritis., Br. J. Rheumatol. 35 (1996) 719–24.

[41] A.S. Williams, Amelioration of rat antigen-induced arthritis by liposomally conjugated methotrexate is accompanied by down-regulation of cytokine mRNA expression, Rheumatology. 40 (2001) 375–383. doi:10.1093/rheumatology/40.4.375.

8 FIGURE CAPTIONS

Figure 1: Schematic representation of the targeting agent and the nanoparticles. (A) Left: schematic representation of the targeting molecule made of a non-correlated ScFv (VL-VH) linked through a hinge to the rat Fc IgG2b (CH2-CH3). In turn, the Fc is fused with an SV5 tag (stripes motif), which ends with the synovial peptide (red). Middle: schematic representation of the synovial peptide, which assumes the circular shape due to the presence of the flanking cysteines. (Red box). Right: 3D model of the targeting molecule modeled with Modeller. The two chains of the dimer are colored in light blue and gold, respectively. In the red boxes the synovial peptide. SDS-PAGE conducted in reducing conditions and analyzed by Coomassie staining (B) and Western Blot (C) of the targeting molecule (lane 1 and 2) show a single band with the expected molecular weight (62 kDa). (D) 3D structure of one monomer of the targeting molecule.

Figure 2: The targeting agent interacts with CD34+ cells in RA inflamed synovial tissue. (A) RA human synovial tissue incubated with the targeting molecule (detected with goat anti-rat Alexa 488) and with anti-vWF (detected with goat anti-rabbit Alexa 594). Nuclei have been stained using Dapi. Scale bar 40 µm. (B) The merge highlights a vessel positive for the vWF and negative for the targeting molecule (red box, scale bar 20 µm), a cell positive for the targeting molecule and negative for the vWF (green box, scale bar 20 µm) and a vessel positive both for the targeting molecule and for the vWF (blue box, scale bar 20 µm). (C) RA human synovial tissues incubated with both the targeting molecule and anti-CD34. Nuclei have been stained with Dapi. From the merge it is possible to observe co-localization between the targeting molecule and the CD34+ cells. Scale bar 40 µm. (D) Merge of the staining performed with the targeting molecule and the anti-CD34 highlights the co-localization (green box, scale bar 20 µm). (E) Untargeted molecule (rat Fc) did not show any staining nor co-localization for the CD34 in RA human synovial tissue.

Figure 3: **Characterization of the nanoparticles.** (A) Left: starting from the top: BNPs with the polymeric shell (blue/grey) made of PEG-b-PLA, PCL and an empty core; tBNPs: identical to the BNPs except for the target molecule linked to the surface; BNPs-MTX: identical to the BNPs but with MTX loaded into the core; tBNPs-MTX: represent the complete format of the nanoparticles, loaded with MTX and provided with the targeting molecule on the surface. Right: schematic representation of the nanoparticles surface with three hypothetical orientations of the targeting molecule exploiting highly solvent accessible primary amines: the protein N-terminus (on Glu1) and the side chains of Lys355 and Lys369 (on the Fc-CH2 domain). The tables summarize the main features of the nanoparticles and the data obtained by NanoTrack (B) and DLS (C) analysis. (D) TEM image of tBNPs (scale bar 100nm). (E) STEM image of tBNPs in dark field (left) and bright

field (right) (scale bar 200nm). (F) Enlargement of the bright field STEM image of the tBNPs (scale bar 100nm). (G) Release studies of MTX from tBNP-MTX in PBS at 37°C for 24h. Samples have been analyzed in triplicate and data reported as the mean ± SD. **** = P ≤ 0.0001 by Two-way ANOVA.

Figure 4: The targeting of nanoparticles enhances binding interaction with endothelial cells. Tracking analysis at 1h (A) and 3h (B) performed on living EA.hy926 cell line incubated with BNPs-Cy5.5 and tBNPs-Cy5.5. Data are expressed as minutes of binding of a single particle and were analyzed by unpaired t-test. ****= P ≤ 0.0001. (C) ELISA test performed on living EA.hy926 cells: tBNPs-FITC and BNPs-FITC have been incubated for 1h with EA.hy926. Data are expressed as intensity of fluorescence at 525nm (mean of 3 biological replicates ± SD) and were analyzed by unpaired t-test. *= P ≤ 0.05. (D) Cropped image obtained by confocal microscopy shows internalized tBNPs-FITC into EA.hy926 cell after 1h of incubation. Scale bars 10μm for XY and 5μm for YZ. (E) Cytotoxicity analysis of EA.hy 926 cell line incubated with free MTX, tBNP-MTX, tBNP-MTX after 24h dialysis or fludarabine (as positive control). Data are presented as % of living cells compared to not treated cells and reported as the mean of biological triplicate ± SD. Statistical significance was calculated with One-way ANOVA multiple comparison test. *=P ≤ 0.05; ****= P ≤ 0.0001.

Figure 5: Biodistribution analysis of BNP and tBNPs in AIA. (A) Images acquired by time domain optical imaging of knees from two representative AIA rats treated i.v. with labeled tBNPs (first rows) and BNPs (second rows). The fluorescence intensity has been reported as normalized counts (NC). (B) Data obtained from 2 groups of rats (n=3) were expressed as mean of fluorescence intensity ± SEM of the right and left paws of the animal. Statistical significance has been tested by two way ANOVA. (C) The graph shows the correlation between swelling (mean ± SEM) and intensity of fluorescence (mean ± SEM) recorded for each paw at day 7. Blue bars represent data from rats treated with tBNPs-Cy5 (n=3), while red bars data from BNPs-Cy5.5 treated rats (n=3). (D) The graph shows ex-vivo fluorescence intensity of main organs (express as mean NC ± SEM). Statistical significance has been tested by unpaired t-test*=P ≤ 0.05; **= P ≤ 0.01; ***= P ≤ 0.001; ****= P ≤ 0.0001;

Figure. 6: Biodistribution analysis of BNP and tBNPs in CIA. (A) Images acquired by time domain optical imaging of two representative CIA mice treated intravenously with tBNPs-Cy5.5 (first panel) or BNPs (second panel), respectively. The score of each paw has been reported on the right of each row. (B) The graphs show the mean intensity of fluorescence (as average radiant efficiency ± SD) detected for a total of 7 days in paws with score 0 or score 3. In this study has been enrolled 7 mice: 4 for tBNPs-Cy5.5 and 3 for BNPs- Cy5.5. The graph regarding the score 0 takes into account n=5 paws of tBNPs-Cy5.5 treated mice and n=7 of BNPs-Cy5.5 treated animals. Instead, the graph of the score 3 takes into account n=4 paw of tBNPs-Cy5.5 treated mice and n=4 of BNPs-Cy5.5 treated animals. Two-way ANOVA multiple comparisons test has been used for statistical analysis. *= P ≤ 0.05; **= P ≤ 0.01; ***= P ≤ 0.001; ****= P ≤ 0.0001. (C) Haematoxylin and Eosin staining of CIA mouse joints with score 0 and 4. In particular, joints usually scored by 0 (no arthritis) by physical examination reveals an initial inflammatory state if analyzed by histology. The initial inflammatory state explains the different fluorescence intensity detected after 1h in mice treated with tBNPs-Cy5.5. Scale bar 100μm.

Figure 7: Effect of tBNP-MTX in CIA. (A) The graph shows arthritic scores of CIA DBA/1 mice treated i.p. with different doses of tBNPs-MTX and free MTX. Groups of mice have been enrolled as follow: saline as control (n=5, red line); MTX 1mg/ Kg three times per week (n=6, continuous

black line); MTX 3mg/Kg once per week (n=4, dotted black line); tBNPs-MTX 3mg/ Kg once per week (n=5, continuous blue line); tBNPs-MTX 1mg/ Kg once per week (n=4, dotted blue line). The scores have been reported as the mean of the sum of the scores ± SEM assessed for each paw of the mouse. Statistical analysis have been assessed by Two-way ANOVA test. *= P ≤ 0.05; **= P ≤ 0.01; ***= P ≤ 0.001; ****= P ≤ 0.0001. (B) Histological images representative of each group of mice treated in this study. An additional image of a healthy paw was added as a negative control. Scale bar 200 μm. (C) The graph represents mice Δ growth in g (weight day 25 – weight day 0) expressed as mean ± SEM. (D) (E) (F) The graphs show WBC, RBC, PLT counts in blood, respectively. Data have been reported as the mean ± SD. Statistical significance has been assessed by t-test. *= P ≤ 0.05; **= P ≤ 0.01.

Figure 8: Effect of tBNP-MTX in AIA and mechanism of action. (A) swelling (diameter day 3 –diameter day 0 in mm) of the inflamed knees and (B) quantification of polymorph nucleated cells detected into synovial fluids from joints of rats treated with saline solution (n=5), 1mg/Kg/day of free MTX (n=4) and 1mg/Kg/day of tBNP-MTX (n=5). A parametric unpaired t-test has been used to assess the statistical significance. (C) vWF staining (Mean fluorescence intensity normalized for the tissue area ± SD) has been determined by ImageJ software. For each animal at least 2 regions of interest (ROIs - showed in Supplementary figure 9) have been analyzed. Number of region of interests (ROIs) analyzed for each group: inflamed=18; tBNPs-MTX=16; MTX= 14; negative CTRL=8. Statistical significance has been assessed using a parametric t-test. *= P ≤ 0.05; **= P ≤ 0.01. (**D**) Schematic representation showing that tBNPs-MTX target endothelial progenitor CD34+ cells. The cytotoxic effect of MTX kills CD34+ cells and prevents the formation of new vessels, which are essential for the whole inflammatory process.

Author contributions: F.C. designed and performed the experiments and wrote the manuscript; P.D. performed and developed and study particles in AIA model; L.D.M. produced targeting agent; S.B. performed optical imaging experiment in rat model; B.B. and C.T. performed and analyzed tissues by histology and immunohistochemistry; R.O. performed in silico study of targeting agent structure and interaction with BNPs; P.B., G.M.M. and E.T. performed and analyzed particle distribution in mouse model; G.P. analyzed mouse blood for toxicological studies; E.R. performed characterized BNPs' structure in vitro; J.B. provided human samples; B.F. performed nanotrack analysis; J.J. and J.A. obtained and analyzed STEM images; L.N. produced BNPs; C.P. contributed with critical revision of the manuscript for important intellectual contents; P.L.M. and F.T. contributed in the design of the study and in the preparation of the manuscript; D.S. designed and contributed to produce the targeting agent; P.M. Designed the study, organized the experiments and the collaborations, wrote the manuscript.

Declaration of interests: Luis Núñez working in Biotarget Inc. and LNK Chemsolutions LLC has commercial interests in the particle systems described in this work. The production of the structure was included in the patent US20070296099 A1.

No conflicts of interest for other authors.

FIGURES

Fig. 1

Fig. 2

Fig. 3

A

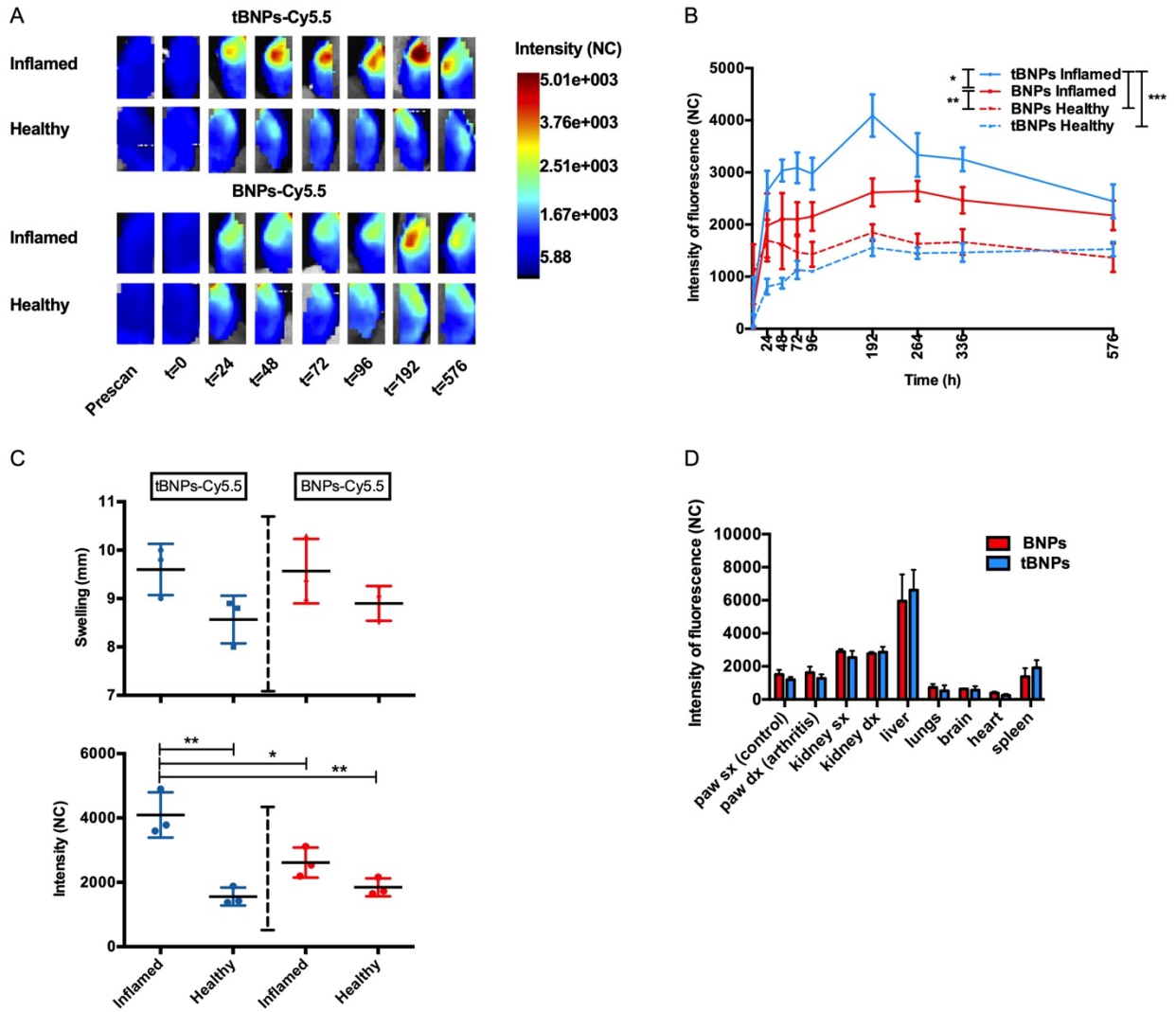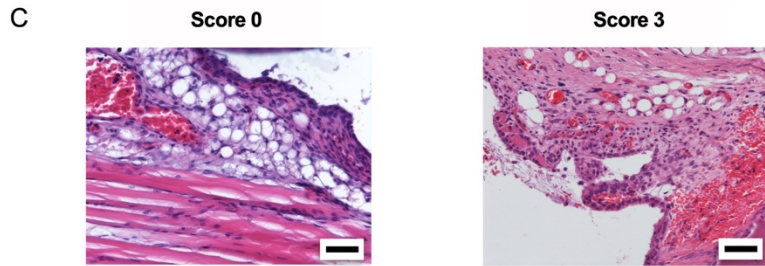BNP

tBNP

BNP-MTX

tBNP-MTX

Lys355

Lys369

Lys369

Glu1

⬜ NHS-COOH-PEG-b-PLA
⬜ COOH-PEG-b-PLA
🔵 COOH-PCL
🟡 Methotrexate

B

Sample	Polymers (mg/mL)	MTX (mg/mL)	Synovial peptide (μg/mL)	Mean diameter (nm)	Particles/mL	PDI
BNPs	1,66	-	-	168	2.5×10^8	0.26
tBNPs	1,66	-	12	164	1.7×10^8	0.24
BNPs-MTX	1,66	2	-	176	3.6×10^8	0.21
tBNPs-MTX	1,66	2	12	160	4.0×10^8	0.21

C

Sample	$d_h \pm SD$ (nm)	PDI	$\zeta \pm SD$ (mV)
BNPs	177 ± 2	0.31 ± 0.02	-9.4 ± 2.9
tBNPs	176 ± 5	0.33 ± 0.04	-6.0 ± 1.4
BNPs-MTX	122 ± 4	0.45 ± 0.07	-9.6 ± 3.6
tBNPs-MTX	139 ± 6	0.36 ± 0.06	-7.1 ± 1.7

D

E

F

G

MTX 2mg/mL
BNPs-MTX 2mg/mL

Fig. 4

A

Tracking analysis 1h

B

Tracking analysis 3h

C

ELISA on EA. hy 926

D

E

Fig. 5

Fig. 6

A

tBNPs-Cy5.5

	1h	6h	24h	72h	96h	168h	Score	Epi-fluorescence
Wrist sx							1	
Wrist dx							1	
Ankle dx							0	
Ankle sx							3	

BNPs-Cy5.5

	1h	6h	24h	72h	96h	168h	Score
Wrist sx							0
Wrist dx							0
Ankle dx							3
Ankle sx							3

Radiant Efficiency
$\left(\frac{p/sec/cm^2/sr}{\mu W/cm^2}\right)$

B

C
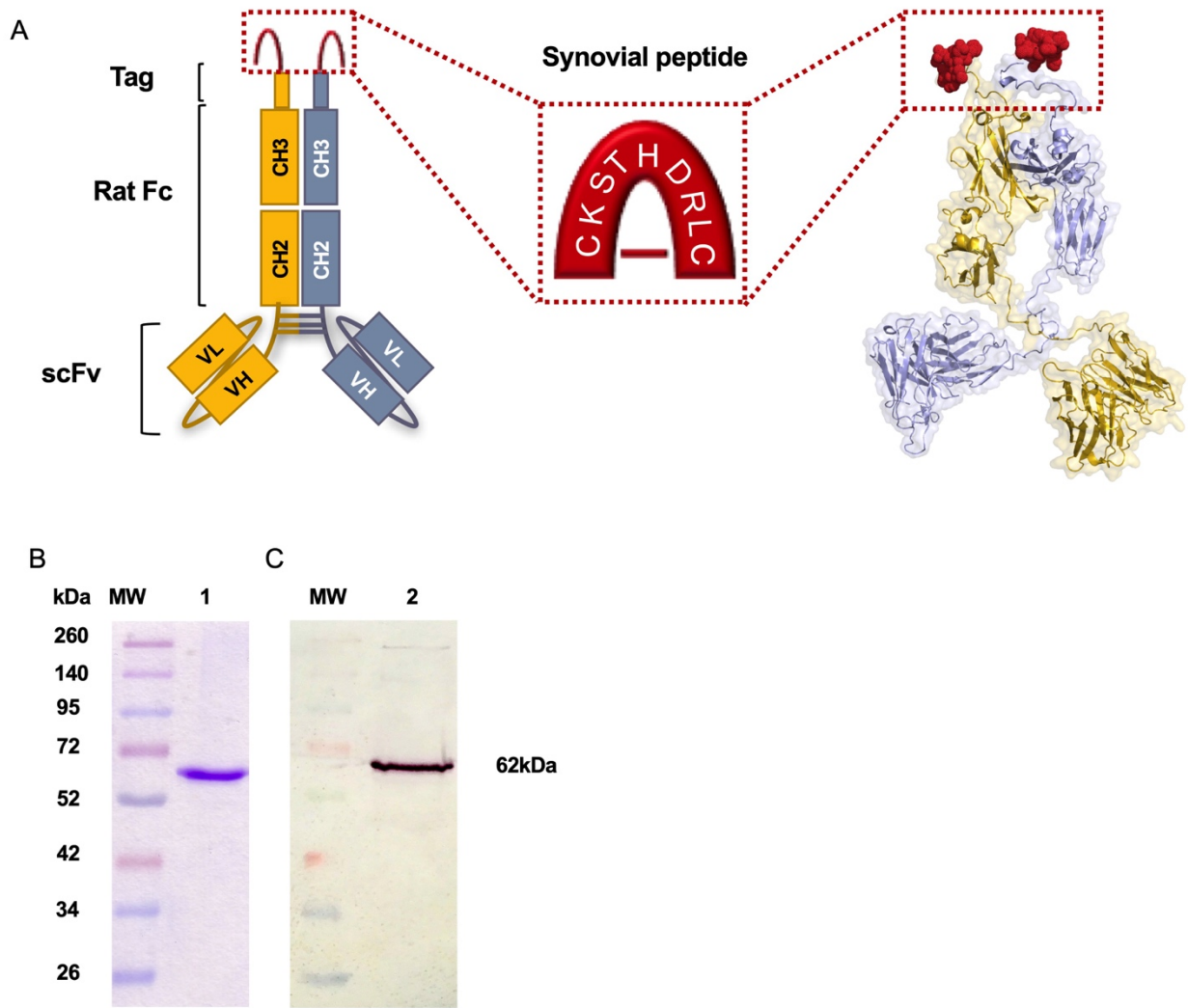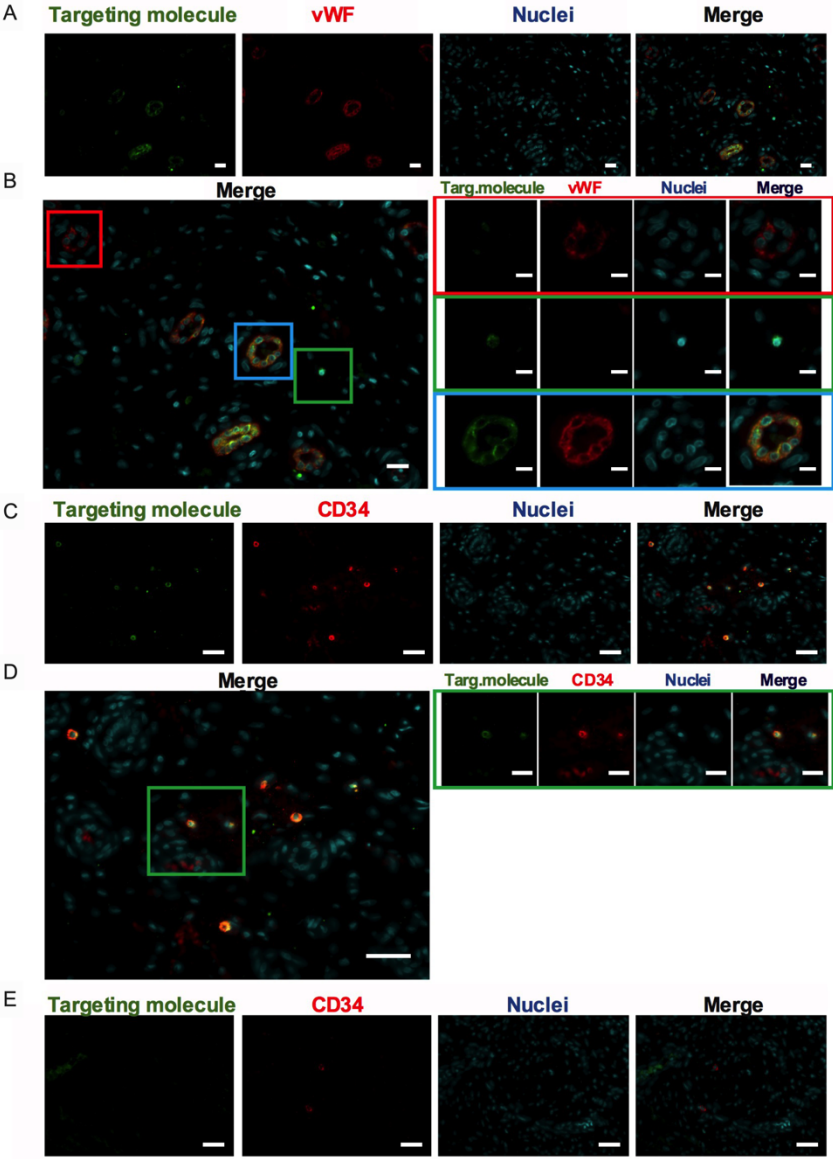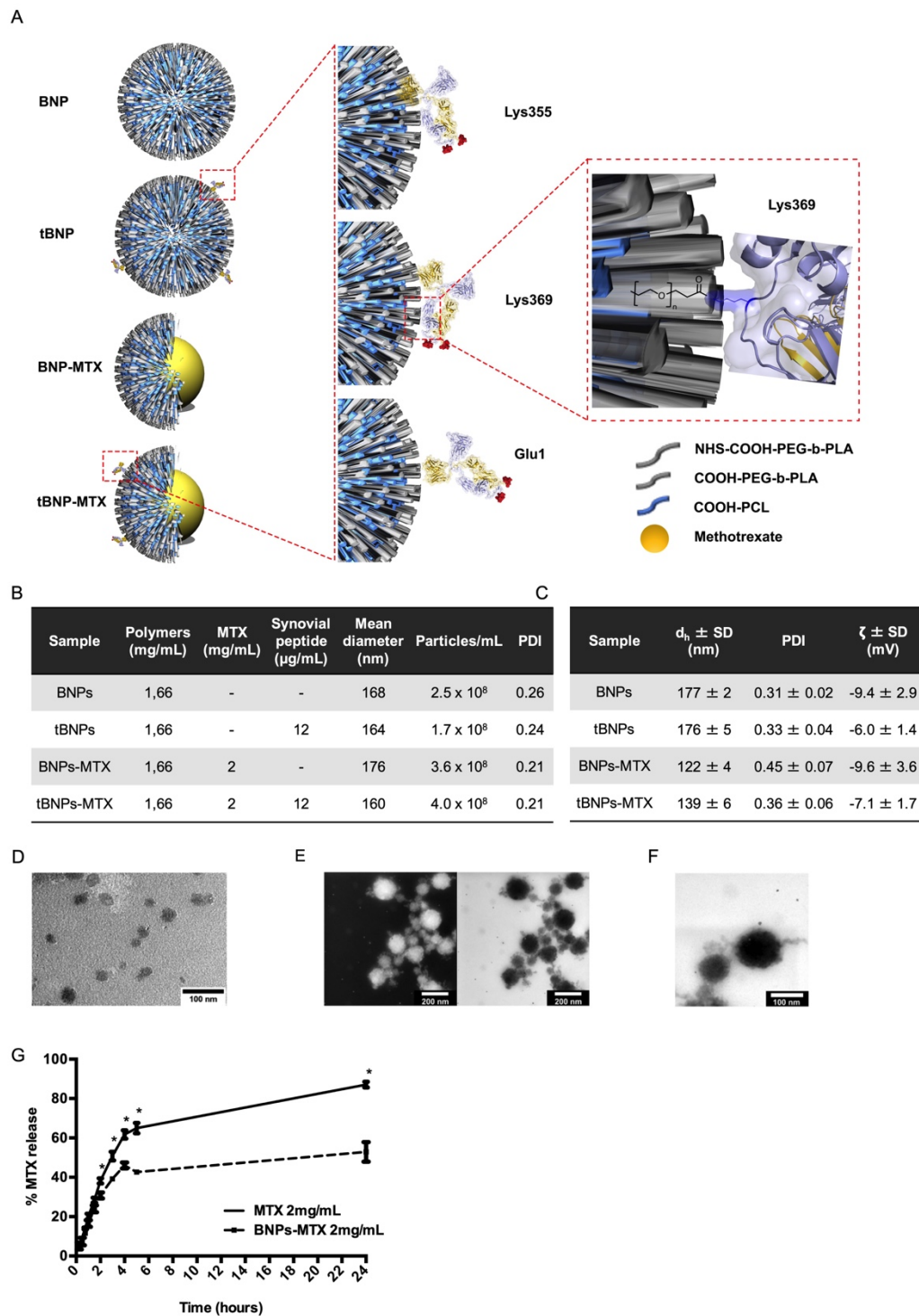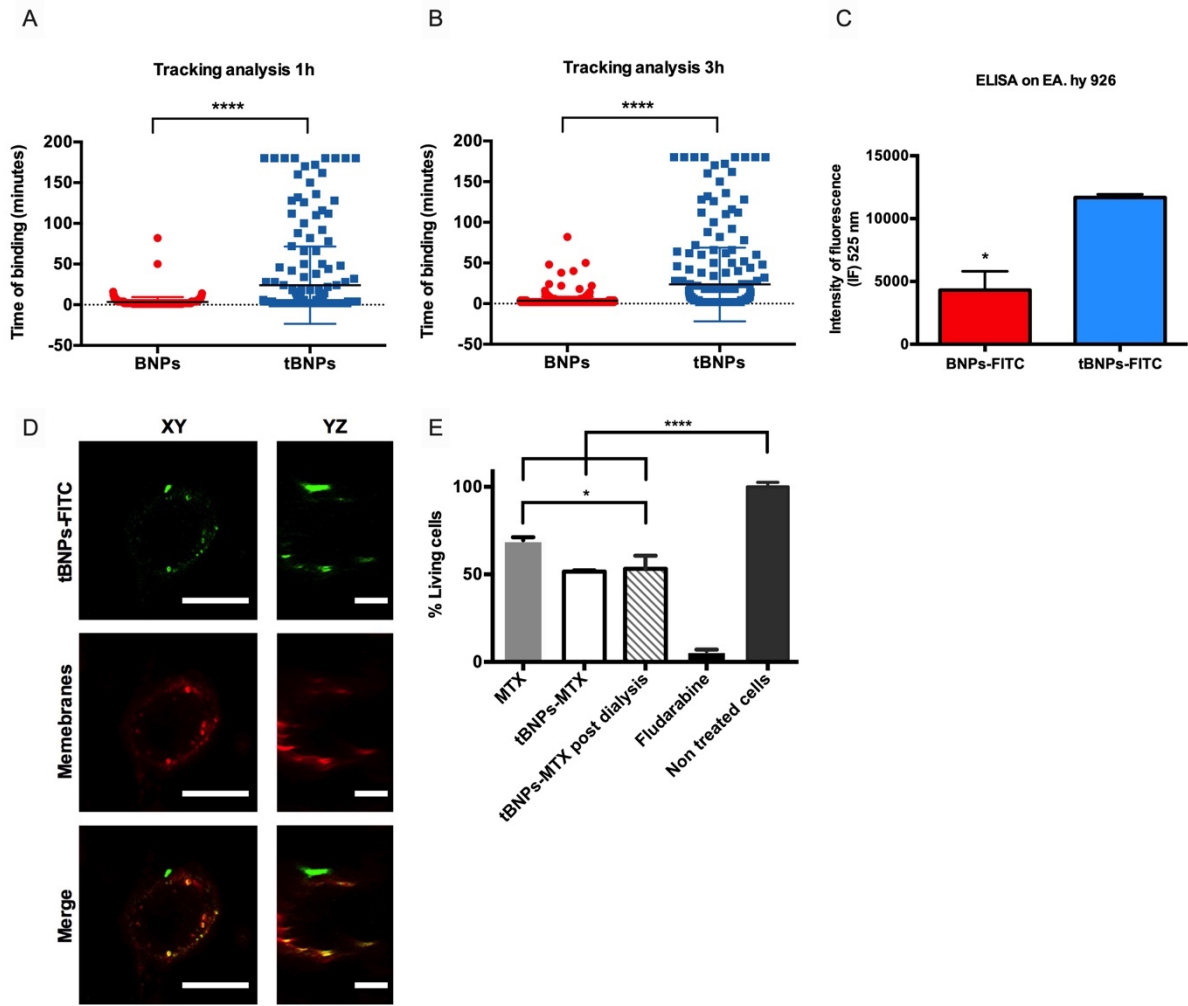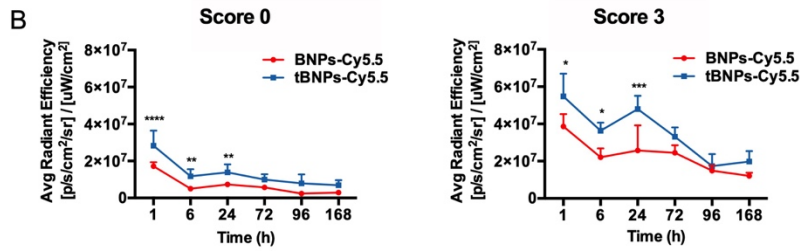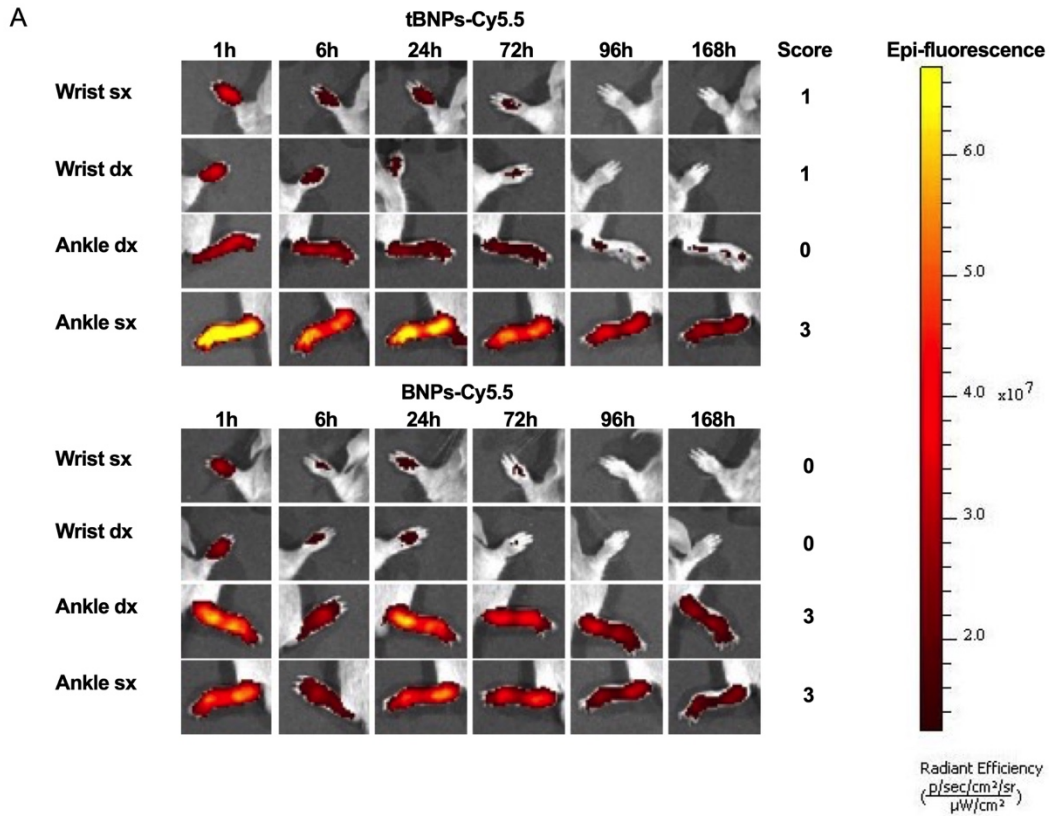
Fig. 7
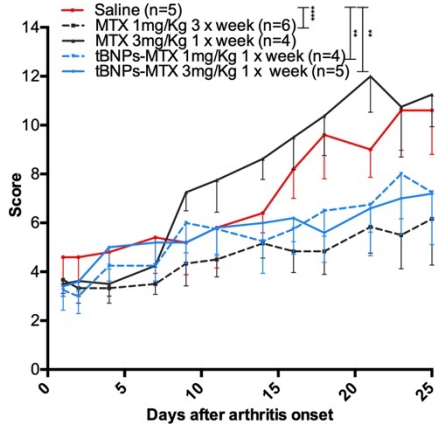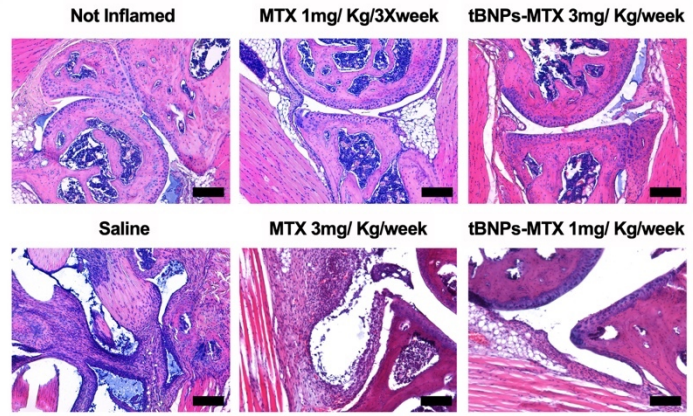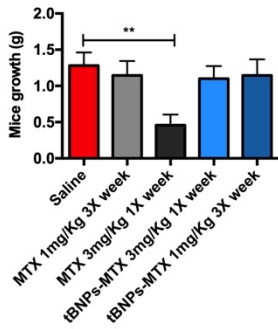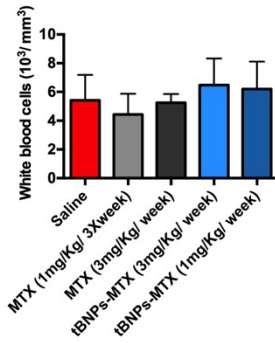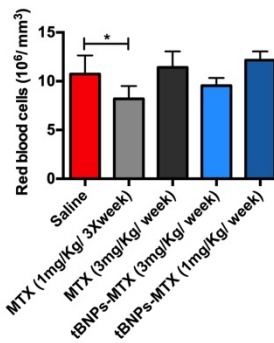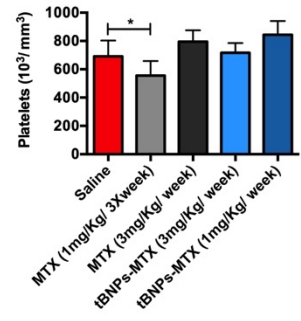
Fig. 8
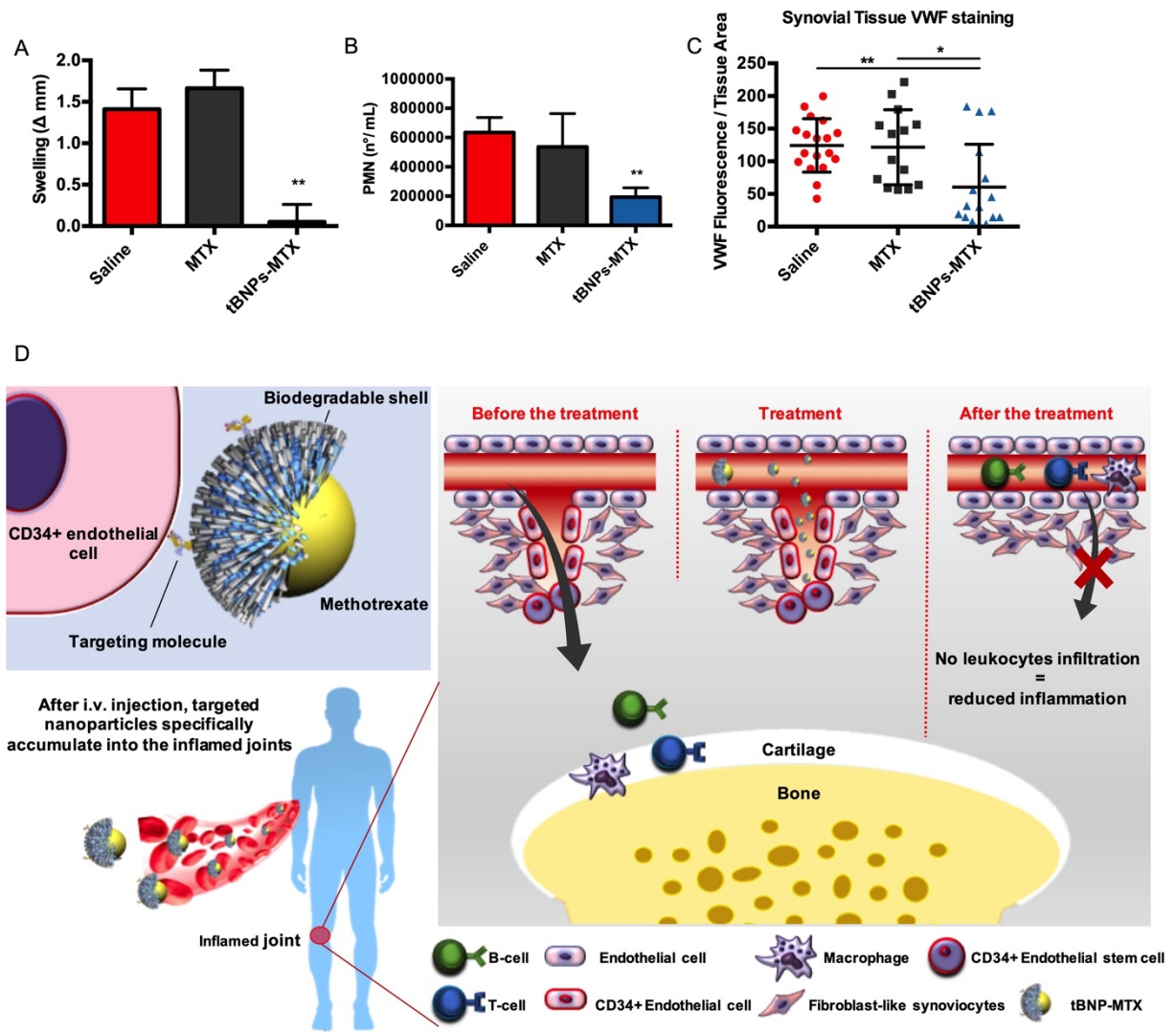
SUPPLEMENTAL INFORMATION (SI)

Supplementary Materials and Methods

Supplementary figures:

Figure S1. The targeting agent selectively binds inflamed rat synovial tissue.

Figure S2. The targeted nanoparticles selectively bind inflamed rat synovial tissue.

Figure S3. Biodistribution studies have been performed in animal groups that uniformly develop AIA.

Figure S4. Histological analysis of synovial tissue from treated mice with CIA.

Figure S5. Analysis of tissue toxicity induced by conventional MTX and tBNP-MTX.

Figure S6. Analysis of blood toxicity induced by conventional MTX and tBNP-MTX.

Figure S7. Efficacy studies have been performed in rat groups with similar immunization and complement activation.

Figure S8. tBNP-MTX reduces neoangiogenesis.

Supplementary videos:

Video S1: Tracking analysis of tBNPs on EA.hy926 cell line.

Video S2: Internalization of tBNPs in EA.hy926 cell line.

Supplementary Materials and Methods

2.1 Design, production and purification of the targeting molecule

The targeting molecule specific for the synovial tissue was generated from a previous scFv-Fc molecule produced and published by our group[1]. This molecule contains the sequence of the scFv specific for C5 of the complement system and the sequence for the hinge-CH2-CH3 domains of rat IgG1 fused to a SV5-tag ending with the synovial peptide (amino acid sequence of the synovial peptide: CKSTHDRLC). To obtain the targeting molecule, the original scFv anti-C5 was substituted with a different scFv (that is unable to cross-react with rat or mouse antigens). Purified plasmid DNA was transfected into Chinese Hamster Ovary cells. The recombinant proteins were purified from the cell medium using a protein A column (Amersham Biosciences, Little Chalfont, UK). The material was dialyzed against PBS and then quantified at 280nm. A schematic figure of the obtained targeting molecule is shown in Fig. 1A.

2.2 Molecular modeling

A 3D model for the dimeric targeting molecule was built with Modeller 9v17[2]. Experimental structures (100% identical in sequence) were available for the scFv domain (PDB ID: 4NYL, resolution 2.8Å) and for the SV5 tag (PDB ID: 5B5L, resolution 1.4Å). CH2 and CH3 domains were modeled by comparative modeling based on a dimeric template with 72% sequence identity (PDB ID: 1IGT, resolution 2.8Å[3]). The 17-residue hinge region connecting CH2 to scFv was modeled based on the hinge region of the same template (1IGT), although the sequence identity dropped to 37% in this region; three cysteine residues of the hinge sequence were aligned to identical residues in the template, thus resulting in the same network of three inter-molecular disulfide bridges. The Gly-rich 16-residue linker between the scFv domains and the 6-residue segment connecting Fc-CH3 to SV5 were modeled by a template-free (ab initio) modeling approach using internal coordinates from the CHARMM topology library. The targeting peptide was modeled based on a structural motif sharing its length and 5 (of 9) identical residues, including the N- and C-terminal Cys (PDB ID: 4GY5, resolution 2.96Å[4]). The model with the lowest value for the Modeller target function among all ten generated models was then subjected to further optimization. The optimization began with a conjugate gradients minimization of up to 300 steps, continued with 2ps of molecular dynamics at 300K, and ended with another conjugate gradients minimization consisting of up to 300 steps. The modeling procedure is summarized in Table S1. Overall, the modeling of the scFv-Fc structure (corresponding to approximately 90% of the molecule) is highly reliable, while the mutual orientation and the orientation of the targeting peptide relative to Fc are tentative. This is due to the lack of good templates and to the intrinsic flexibility of the two connecting segments (the hinge between scFv and Fc and the Fc-tail between Fc and the SV5 tag).

The relative solvent accessibility (RSA) of the model, calculated by NACCESS[5], showed that the side chains of the 50 Lys residues (25 per chain) are highly exposed to the solvent (side chain RSA above 40%), with Lys355 and Lys369 featuring the highest side-chain accessibility (RSA ≈ 100%). As expected, the main chain, and therefore the amino group of the N-terminal Glu1 residue, are also highly solvent accessible (main chain RSA ≈ 100%).

Table S1. Main features of the modeling process.

Domain/Fragment	Residues	Template	Technique	Sequence identity (%)
scFv-heavy chain	1-121	4NYL	Transfer of coordinates	100
Linker	122-137	-	Template-free modeling	-
scFv-light chain	138-244	4NYL	Transfer of coordinates	100
Hinge	245-261	1IGT	Comparative modeling	37[a]
Fc-CH2	262-370	1IGT	Comparative modeling	82
Fc-CH3	371-472	1IGT	Comparative modeling	61
Fc-tail	473-478	-	Template-free modeling	-
SV5	479-492	2B5L	Transfer of coordinates	100
Targeting peptide	493-501	4GY5	Comparative modeling	47[a]

[a] A relatively high target-to-template sequence identity measured on a short segment does not necessarily imply structural similarity[6].

2.3 Dynamic light scattering (DLS) and ζ-potential analysis

A Malvern Nano ZS instrument (Malvern Panalytical Ltd, Malvern, UK) equipped with a 633nm laser diode. NP hydrodynamic diameter (dH) distributions were obtained in PBS at 25°C. Samples were filtered with 0.45µm RC filters and then housed in disposable polystyrene cuvettes (1 cm optical path length). The average width of the DLS hydrodynamic diameter distribution is indicated by the PdI: in cases of a mono-modal distribution (Gaussian), PdI is calculated by means of cumulant analysis, PdI=$(\sigma/Zavg)2$, where σ is the width of the distribution, and Zavg is average diameter of the particle population. The hydrodynamic diameter standard deviation (SD) was calculated over five different measurements.

The DLS technique over-weights the average size for a colloidal sample with moderate polydispersity (PdI>0.2): for this reason, we showed the size distribution by number to represent a more realistic picture of the average hydrodynamic diameter of the sample.

Electrophoretic determination of the ζ-potential was made under the Smoluchowski approximation in single mode conditions using a fast field reversal (FFR) measurement. This measurement mode allowed a more accurate determination of the ζ-potential mean value for each NP sample

2.4 Nanoparticle tracking analysis (NTA)

NTA measurements were performed with a NanoSight LM10 instrument (NanoSight, Amesbury, UK) according to the manufacturer's instructions. A short video of 60 seconds per sample was acquired and then analyzed by NTA 2.0 Analytical software. Each sample was analyzed in triplicate.

2.5 Transmission electron microscopy (TEM) analysis

TEM images of NP samples were obtained with a Philips CM 100 microscope (Guildford, UK) operating at 80kV and using 3.05 copper grids (Formvar support film – 400 mesh). A drop of NP water suspension was placed on the grid and then dried under a vacuum.

2.6 Scanning transmission electron microscopy (STEM) analysis

The sample suspension was dispersed over the TEM grid and air dried. All specimens were examined with a field emission scanning electron microscope (MAIA3 Tescan, Brno, Czech Republic) using a STEM detector. Bright field (BF) and dark field (DF) images were obtained simultaneously with an accelerating voltage of 30kV.

2.7 MTX release from tBNPs

To evaluate the amount of MTX released from nanoparticles, 200μL of tBNPs-MTX were dialyzed (molecular weight cut-off: 3.5kDa) against 10mL of PBS at 37°C. Dialysis solution was collected for each time point and the optical density was measured at 320nm by an Infinite M200 Pro plate reader (Tecan, Männedorf, Switzerland). The $OD_{320 nm}$ of MTX (2mg/mL diluted in 10mL of PBS) was used as the 100% reference value. Then, the percentage of MTX release was calculated as follows: (OD_{320} sample x 100)/OD_{320} 100% MTX. Each sample was analyzed in biological triplicates for each time point.

2.8 MTT viability assay with EA.hy926 cells

EA.hy926 cells were cultured in a 96-well cell culture plate (Sarstedt, Nümbrecht, Germany) at 37°C with 5% CO_2 in Dulbecco's Modified Eagle's Medium (DMEM) supplemented with 10U/mL penicillin, 1 μg/mL streptomycin, 2 mM L-glutamine and 10% FBS (Sigma, Milan, Italy). Cells were incubated for 48 hours with free MTX (9nM), MTX (9nM) loaded into tBNPs, tBNPs dialyzed for 24 hours, or Fludarabine (28nM)(Mylan, Canonsburg, PE, USA). Residual cell viability was evaluated by an MTT assay, and the percentage of viable cells was calculated using untreated cells as the 100% viable cells reference.

2.9 SDS-PAGE and Western blot

The targeting molecule (1μg) was analyzed by SDS-PAGE in reducing conditions. The gel was analyzed using Coomassie Brilliant Blue R-250 (Sigma). Western blot analysis was then performed and proteins were analyzed using an anti-SV5 mAb and phosphatase-labeled anti-mouse secondary antibody.

2.10 Labeling the targeted molecule

The targeting molecule was labeled with a near-infrared probe, FluoroLink Cy5.5 Monofunctional Dye (GE Healthcare), following the manufacturer's instructions.

2.11 Labeling the nanoparticles

Nanoparticles (1mg of polymers) were resuspended in 500μL of sodium carbonate buffer pH9.3. Then, 50μL of FITC (1mg/mL in DMSO) (Sigma) was incubated overnight with the particles at 4°C. Repeated centrifugation steps were used to eliminate unbound dye. Using the same method, nanoparticles were labeled with the near-infrared probe FluoroLink Cy5.5 Monofunctional Dye (GE Healthcare). The amount of Cy5.5 or FITC associated with the nanoparticles was quantified by spectrophotometric methods.

2.12 Hematoxylin & eosin staining

Excised organs and joints were fixed in 10% neutral buffered-formalin and embedded in paraffin. Subsequently, sections (4μm) were cut and stained with hematoxylin-eosin for histopathological analyses performed by two pathologists with specific expertise in mouse pathology.

Histopathological scoring of autoimmune tissue damage in the joints was obtained by evaluating and scoring the following variables: synovial/stromal proliferation, lymphoid/granulocytic inflammatory infiltration, cartilage/subchondral bone infiltration and remodeling, and fibrinoid necrosis. All the variables were scored as follows: 0, absent; 1, focal/mild; 2 multifocal/moderate; and 3 diffuse/severe. The final damage score for each case was calculated by summing the individual variable scores for that case.

In all the animal groups, morphological analysis of various organs including the spleen, brain, lungs, heart, kidneys, and liver was performed to assess tissue damage related to treatment toxicity. Slides were evaluated under a Axioscope A1 microscope (Zeiss).

2.13 Blood analysis

Blood samples collected from rats and mice were analyzed to assess the numbers of red blood cells, white blood cells and platelets using an ABX Micros ES60 (Horiba ABX Diagnostics, Montpellier, France) according to the manufacturer's instructions.

2.14 Number of PMN leukocytes

To measure the number of PMN leukocytes in synovial washes of AIA rats, the myeloperoxidase activity was measured. For this purpose, a standard curve using rat PMN was prepared. The sample (100μL) was loaded in a 96-well plate (Corning, NY, USA), and TMB (Sigma) was added. The colorimetric reaction was stopped with 1M H_2SO_4 (Sigma) and measured by an Infinite M200 Pro (Tecan).

2.15 Binding of nanoparticles to EA.hy926

Ea.hy926 cells were seeded in a 96-well cell culture plate (Sarstedt) and cultured in DMEM with 10U/mL penicillin (Sigma), 1μg/mL streptomycin (Sigma), 2mM L-glutamine (Sigma) and 10% FBS. Cells were then fixed with 1% PFA for 30 minutes at RT and blocked with 1% BSA in PBS. BNPs-FITC and tBNPs-FITC (2.4μL in 100μL of 30% FBS in PBS) were incubated with cells for 1 hour at 37°C.

The intensity of fluorescence obtained from bound particles was detected with a FLUOstar Omega microplate reader (BMG Labtech, Ortenberg, Germany) at 520 nm.

Additionally, cells were fixed with 4% PFA, nuclei were stained with DAPI (4',6-diamidin-2-phenylindole)(Sigma) and samples were mounted with Mowiol anti-fade medium (Polyscience Inc., Warrington, PA).

2.16 Tracking analysis

EA.hy926 cells were cultured in an X-well Tissue Culture Chamber (Sarstedt) at 37°C with 5% CO_2 in supplemented DMEM. The analysis was conducted with the Nikon Eclipse Ti-E Live Cell Imaging System (Nikon). Fluorescent BNPs and tBNPs were incubated with cells. Each video was obtained by acquiring frames (area=360.00x239.41μm) every 2 minutes for a total of 3 hours (91 frames). The interactions between the cells and the nanoparticles were calculated by TrackMate plugin FIJI[7]. TrackMate's filters were adjusted manually and applied in order to exclude artifacts, cell debris, non-round particles or objects with a diameter greater than 2μm.

2.17 Preparation and staining of paraffin embedded sections of human synovial tissues

Paraffin embedded synovial tissues were obtained from RA patients with their consent. Sections (7µm) were cut by a microtome hyrax m55 (Carl Zeiss), dried for 2 hours at RT and baked at 55°C for 2 hours. Slices were de-waxed by immersion in xylene, followed by 100% ethanol, 96% ethanol, 80% ethanol and 70% ethanol. Then, slides were rehydrated in distilled H_2O for 2 minutes and then incubated in TBS for 2 minutes. Antigen retrieval was performed enzymatically with a solution of 0.05% trypsin and 0.5% CaCl2 in distilled H_2O at 37°C for 20 minutes. Afterward, the slices were washed with distilled H_2O and blocked for 30 minutes at RT in a humid chamber with 2% serum of the animal in which the secondary antibody was developed in PBS. The excess blocking buffer was removed, the primary antibody was added at O/N 4°C in 0.2% BSA and 0.05% Tween20 in PBS. After washing with 1% of Triton 100x in PBS, a secondary antibody conjugated to a fluorescent probe and diluted was added for 1 hour at RT. Nuclei were stained with DAPI diluted in PBS for 5 minutes at RT. Finally, the slices were mounted with Mowiol (Polysciences).

2.18 Staining with the targeting molecule

The targeting molecule (10µg/mL) was incubated O/N at 4°C and then detected with a goat anti-rat Alexa 488 (A-11006-Invitrogen, 1:200)

2.19 Staining of vWF

A rabbit anti-vWF antibody (A0082-Dako, Santa Clara, CA, USA, 1:400) was used then recognized by a goat anti-rabbit antibody Alexa 594 (A-11037-Invitrogen, 1:200).

2.20 Staining of CD34+

A rabbit anti-CD34 antibody (bs-0646R-Bioss, Woburn, MA, USA, 1:200) was used, then recognized by a goat anti-rabbit antibody Alexa 594 (Invitrogen).

2.21 Staining of frozen sections with antibodies

Tissues collected from AIA rats were included in Tissue TEK OCT (BioOptica) and were then frozen at -80°C. Sections (7µm) were cut by a cryostat Leica CM 3050 S (Leica, Wetzlar, Germany) equipped with a microtome. Sections were dried O/N at RT and then stored at -20°C. Before their use, the sections were rehydrated with 0.9% NaCl. Samples were blocked with 2% of the animal serum (in which the secondary antibody was developed) in PBS for 30 minutes at RT in a humid chamber. Sections were incubated with the primary antibody in 0.2% BSA and 0.05% Tween20 in PBS and washed with 1% Triton X-100 in PBS. The secondary antibody was added for 1h. Nuclei were stained with DAPI, and the slices were mounted with Mowiol (Polyscience).

2.22 Staining with the targeting molecule

The targeting molecule (10µg/mL), previously conjugated to Cy5.5 was incubated O/N at 4°C.

2.23 Staining of vWF

A rabbit anti-vWF (A0082-Dako, 1:4009 was used then recognized with a goat anti-rabbit-AlexaFluor 594 antibody (Invitrogen)

2.24 Staining of C3

A goat anti-C3 (Cappel, 1:50) was used followed by a rabbit anti-goat-TRITC antibody (T7028-Sigma, 1:100).

2.25 Staining of frozen sections with nanoparticles

Sections were rehydrated with 0.9% NaCl and blocked with universal blocking buffer (2% BSA, 0.25% Casein from bovine milk (Sigma) and 0.10% gelatin from porcine skin (Sigma) in PBS) for 30 minutes at RT in a humid chamber. BNPs-FITC or tBNPs-FITC were then incubated for 1 hour at 37°C. Finally, slices were mounted with Mowiol (Polyscinece).

2.26 Fluorescence microscopes used in this work

Zeiss AxioPlan 2 Microscopy System (Carl Zeiss, Oberkochen, Germany) equipped with an AxioCamHR3 camera.
Nikon Eclipse Ti-E Live Cell Imaging System (Nikon, Amsterdam, Netherlands) equipped with a Nikon DS-Qi2 camera and stage incubation system able to control temperature, humidity and percentage of CO_2.
Nikon C1-SI confocal microscope (TE-2000U)(Nikon) equipped with 20x and 60x oil immersion lenses and a pinhole of 30nm.
Post processing of the images was conducted with FIJI (ImageJ) software.

Supplementary bibliography
[1]   P. Macor, P. Durigutto, L. De Maso, C. Garrovo, S. Biffi, A. Cortini, F. Fischetti, D. Sblattero, C. Pitzalis, R. Marzari, F. Tedesco, Treatment of experimental arthritis by targeting synovial endothelium with a neutralizing recombinant antibody to C5, Arthritis Rheum. 64 (2012) 2559–2567. doi:10.1002/art.34430.
[2]   Andrej Šali, MODELLER A Program for Protein Structure Modeling, Comp. Protein Model. by Satisf. Spat. Restraints. (1993) 779–815. doi:10.1006/jmbi.1993.1626.
[3]   L.J. Harris, S.B. Larson, K.W. Hasel, A. McPherson, Refined structure of an intact IgG2a monoclonal antibody, Biochemistry. 36 (1997) 1581–1597. doi:10.1021/bi962514+.
[4]   J. Cheng, Y. Yang, J. Fang, J. Xiao, T. Zhu, F. Chen, P. Wang, Z. Li, H. Yang, Y. Xu, Structural insight into coordinated recognition of trimethylated histone H3 lysine 9 (H3K9me3) by the plant homeodomain (PHD) and tandem tudor domain (TTD) of UHRF1 (ubiquitin-like, containing PHD and RING finger domains, 1) protein, J. Biol. Chem. 288 (2013) 1329–1339. doi:10.1074/jbc.M112.415398.
[5]   J.M.T. Simon J Hubbard, Naccess, Comput. Program, Dep. Biochem. Mol. Biol. Univ. Coll. London. 2 (1993).
[6]   C. Sander, R. Schneider, Database of homology-derived protein structures and the structural meaning of sequence alignment, Proteins Struct. Funct. Bioinforma. 9 (1991) 56–68. doi:10.1002/prot.340090107.
[7]   J.Y. Tinevez, N. Perry, J. Schindelin, G.M. Hoopes, G.D. Reynolds, E. Laplantine, S.Y. Bednarek, S.L. Shorte, K.W. Eliceiri, TrackMate: An open and extensible platform for single-particle tracking, Methods. 115 (2017) 80–90. doi:10.1016/j.ymeth.2016.09.016.

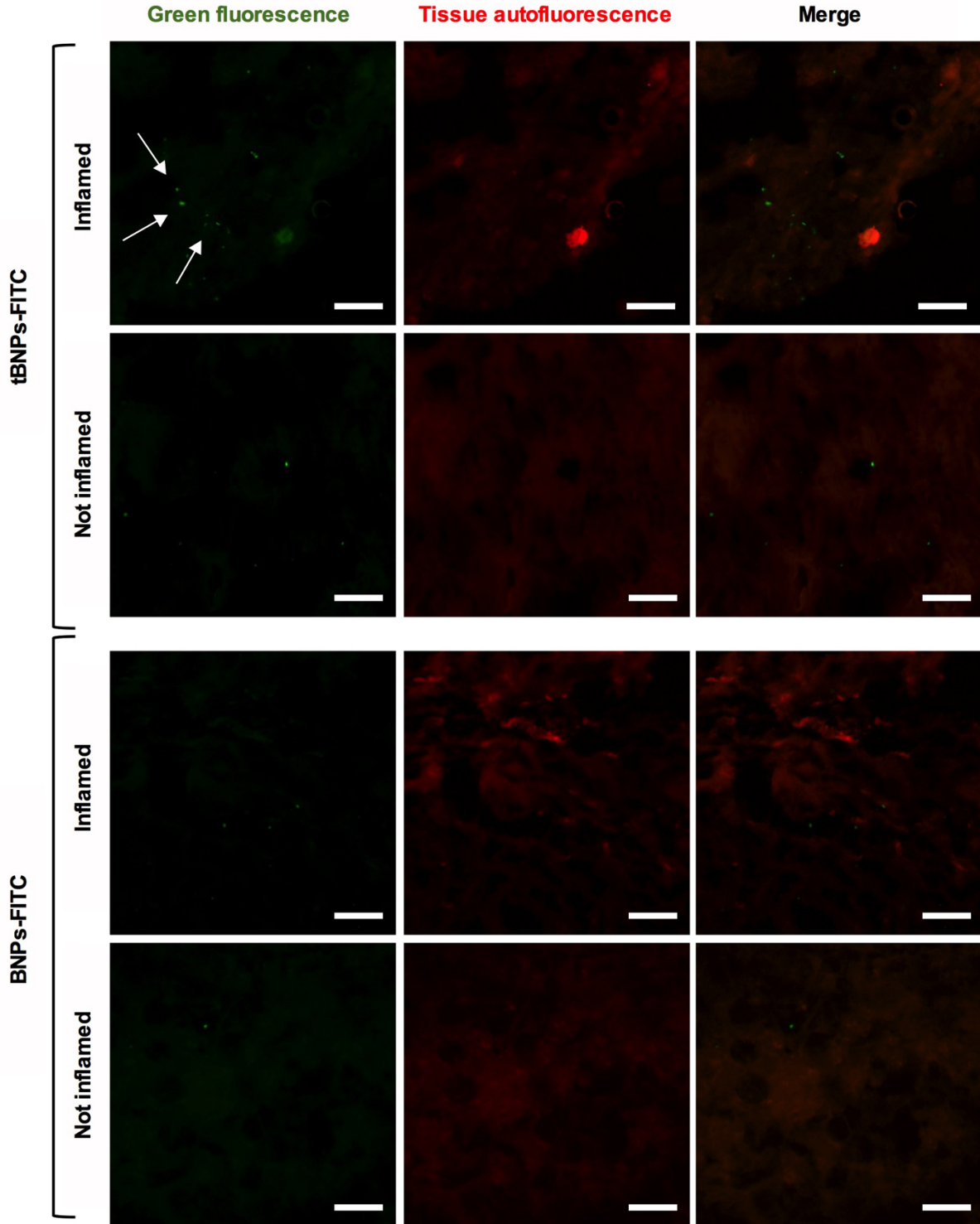**Supplementary figures**

Fig. S1
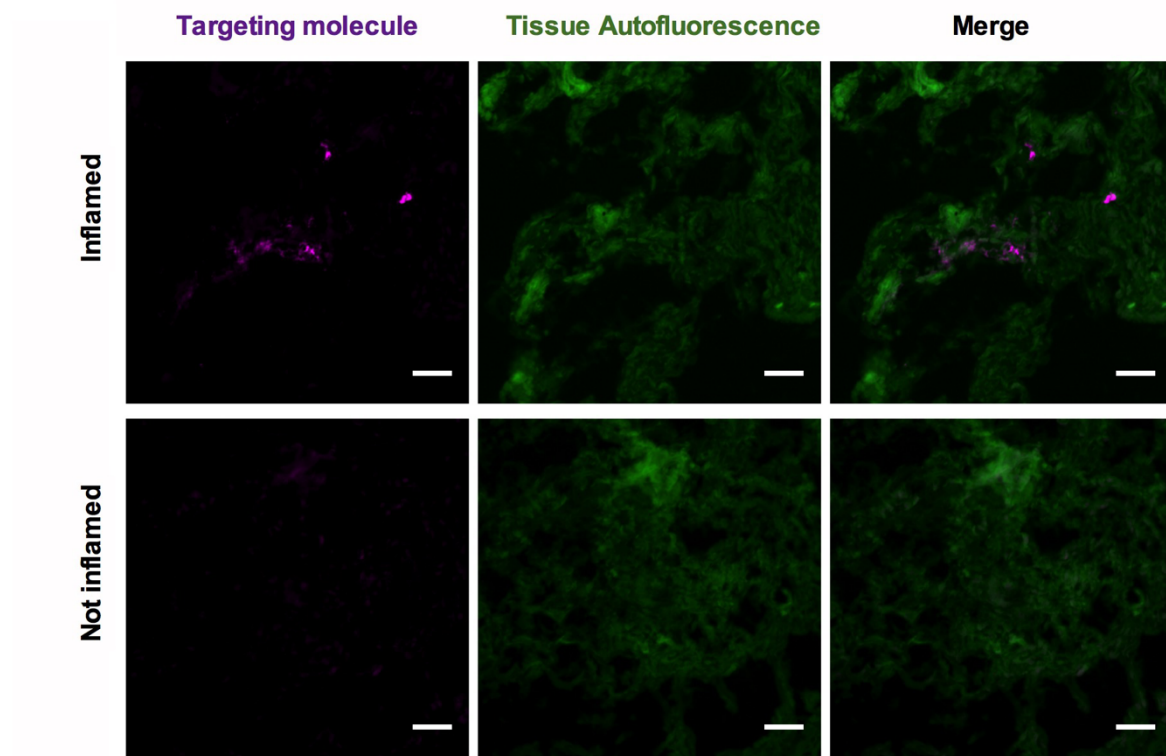
Figure S1: The targeting agent selectively binds inflamed rat synovial tissue. Inflamed and healthy synovial tissue of AIA rats (green autofluorescence) were incubated with targeting molecule-Cy5.5 (magenta). Scale bar 50 μm.

Fig. S2

Figure S2: The targeted nanoparticles selectively bind inflamed rat synovial tissue. Inflamed and healthy synovia from AIA rats (red autofluorescence) were incubated with tBNP-FITC and BNPs-FITC and visualized by fluorescent microscopy (white arrows). Scale bar 50 μm.
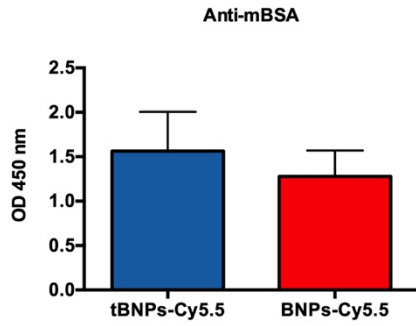
Fig. S3

Figure S3: Biodistribution studies have been performed in animal groups that uniformly develop AIA. In order to evaluate the immune response of rats used for the study of biodistribution, the presence of anti-mBSA antibodies has been detected by ELISA test into serum samples of animal treated with tBNPs and BNPs.

Fig. S4
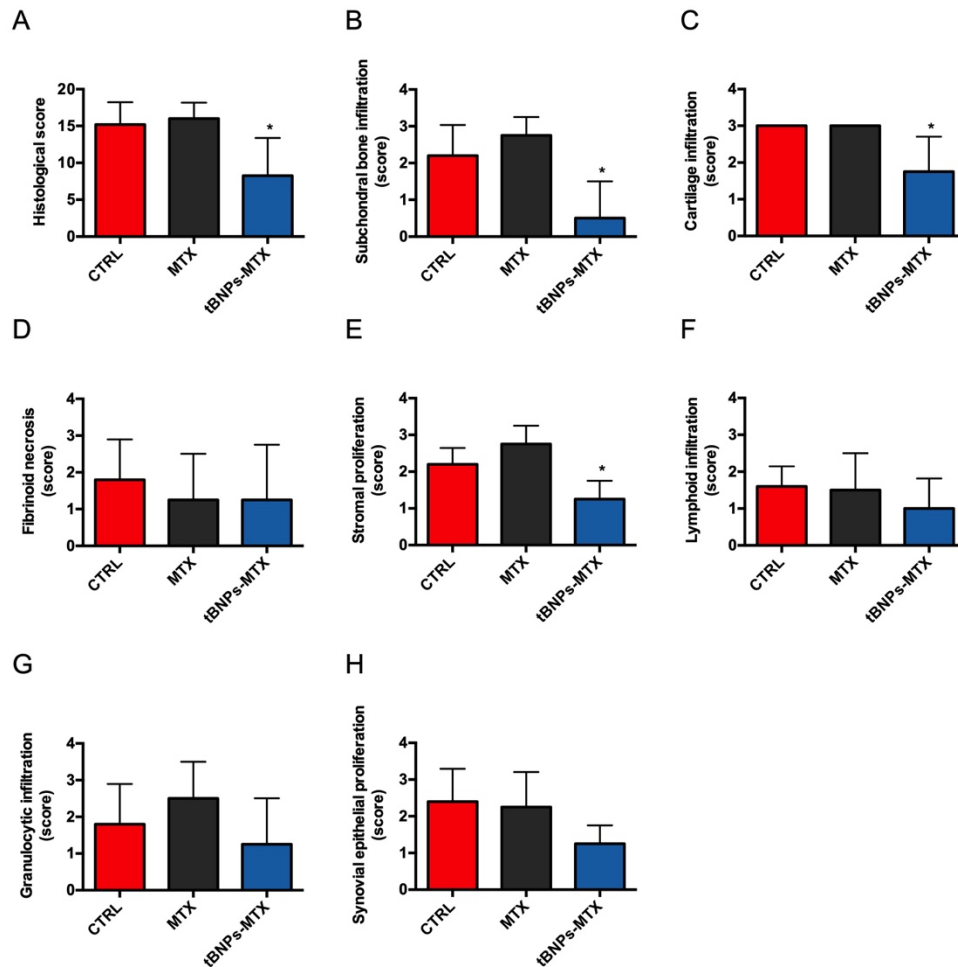
Figure S4: Histological analysis of synovial tissue from treated mice with CIA. (A) Histological total score reported as the mean ± SD of values assigned for each CIA mouse. Seven different parameters have been taken into account: subchondral bone infiltration (B), cartilage infiltration (C), fibrinoid necrosis (D), stromal proliferation (E), lymphoid infiltration (F), granulocytic infiltration (G) and synovial epithelial proliferation (H). Statistical significance has been assessed by unpaired t-test. *= P ≤ 0.05.
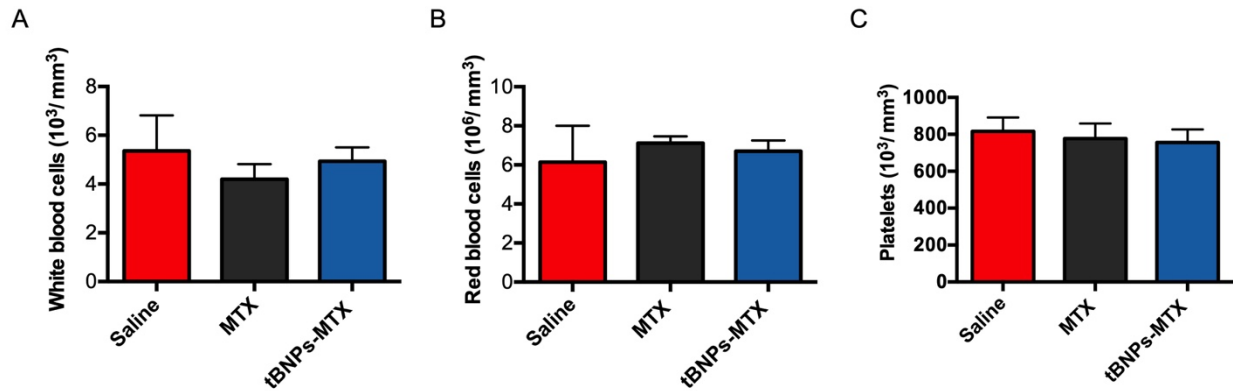
Fig. S5
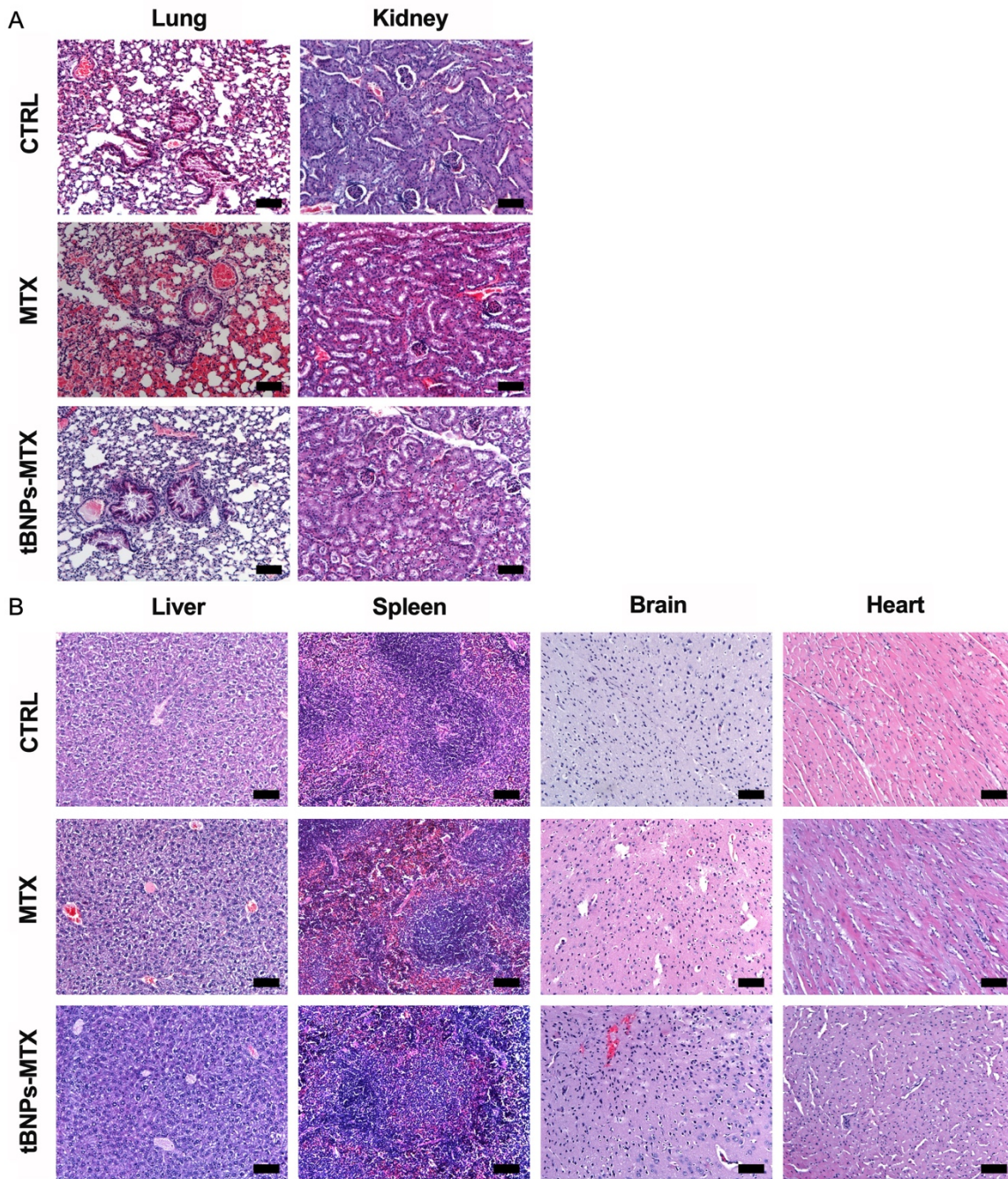
Figure S5: Analysis of tissue toxicity induced by conventional MTX and tBNP-MTX. Representative microphotographs showing disarray of the mouse lung and kidney parenchyma (A) and no significant histopathological alteration of liver, spleen, brain and heart (B). Scale bar 200 μm
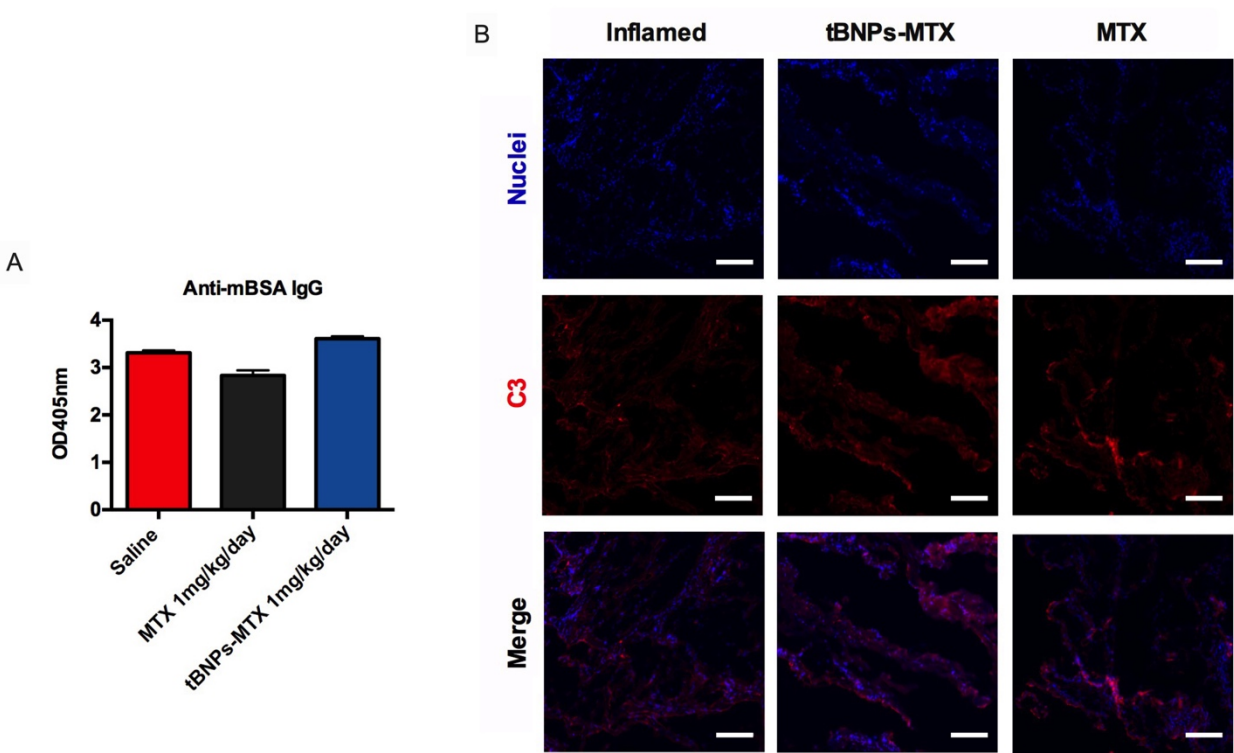
Fig. S6

A

B

C

Figure S6: Analysis of blood toxicity induced by conventional MTX and tBNP-MTX. Rats treated with saline solution (n=5), MTX (n=4) and tBNP-MTX (n=5). White blood cells (A), red blood cells (B) and platelets (C) have been quantified at the end of the study. Data have been reported as the mean ± SD. Statistical significance has been assessed by t-test. *= P ≤ 0.05.

Fig. S7

Figure S7: Efficacy studies have been performed in rat groups with similar immunization and complement activation. (A) Evaluation of anti-mBSA IgG in sera of rats treated with saline, MTX and tBNPs-MTX by ELISA. Data are shown as the mean ± SD of a biological triplicate of pooled sera for each group of rats. (B) Immunofluorescence staining of C3 complement component on the inflamed synovial tissue of treated rats (red fluorescence) and nuclei with DAPI. Scale bar 100 μm.

Fig. S8
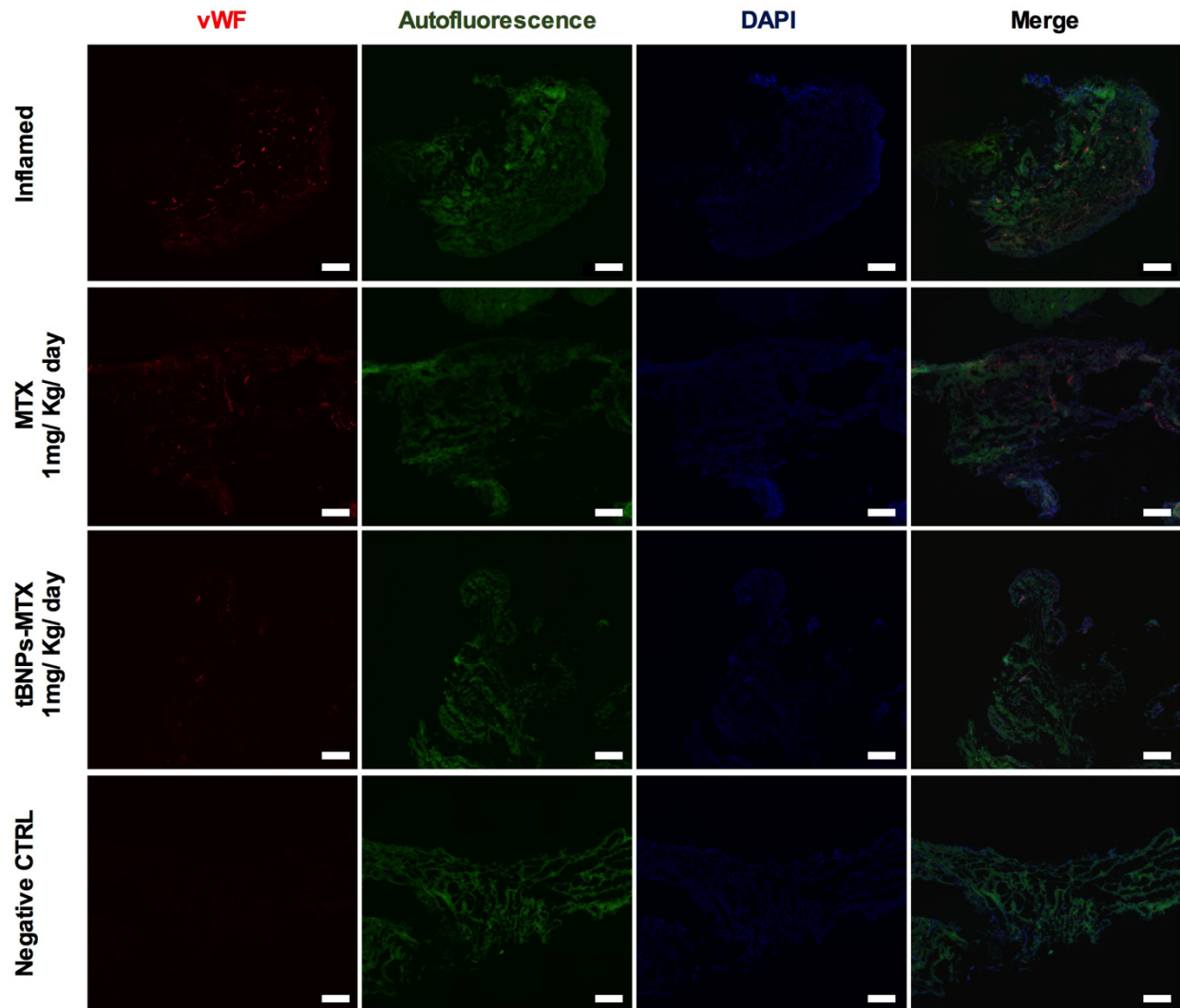
Figure S8: tBNP-MTX reduces neoangiogenesis. Immunofluorescence staining for the evaluation of vWF on the inflamed synovial tissue of rats treated with saline solution, tBNPs-MTX or conventional MTX has been performed using anti-vWF detected with goat anti-rabbit Alexa 594. Non-inflamed synovial tissues have been used as negative control. Nuclei have been stained with Dapi. In order to evaluate a large area of tissues, each image is a large field obtained through the stitching of 9 images. Scale bar 200 μm. Quantitative data have been reported in the Fig. 8C.

Video captions:

Video S1: Tracking analysis of tBNPs on EA.hy926 cell line. The video shows the incubation of EA.hy926 cells with 1μL tBNPs-Cy5.5 for a total of 3h. Each frame of the video has been taken every 2 minutes in fluorescence and bright field. The fluorescence channel of the video has been used to calculate the tracking path of the particles incubated with the cells by using the TrackMate plugin of FIJI

Video S2: Internalization of tBNPs in EA.hy926 cell line. Confocal microscopy Z-stacks reconstruction of a EA.hy926 cell incubated with tBNPs for 1h. The cell membranes have been stained with a red fluorescence. This animation shows that tBNPs-FITC merge with membranes of the cell, demonstrating their internalization.